

# Artificial Intelligence-based algorithms in medical image scan segmentation and intelligent visual-content generation - a concise overview

Zofia Rudnicka, Janusz Szczepanski, Agnieszka Pregowska\*

Institute of Fundamental Technological Research, Polish Academy of Sciences, Pawinskiego 5B, 02-106 Warsaw, Poland  
\* Correspondence: arego@ippt.pan.pl; Tel.: +48-22-826-1281 (ext. 412)

**Abstract:** Recently, Artificial Intelligence (AI)-based algorithms have revolutionized the medical image segmentation processes. Thus, the precise segmentation of organs and their lesions may contribute to an efficient diagnostics process and a more effective selection of targeted therapies as well as increasing the effectiveness of the training process. In this context, AI may contribute to the automatization of the image scan segmentation process and increase the quality of the resulting 3D objects, which may lead to the generation of more realistic virtual objects. In this paper, we focus on the AI-based solutions applied in the medical image scan segmentation, and intelligent visual-content generation, i.e. computer-generated three-dimensional (3D) images in the context of Extended Reality (XR). We consider different types of neural networks used with a special emphasis on the learning rules applied, taking into account algorithm accuracy and performance, as well as open data availability. This paper attempts to summarize the current development of AI-based segmentation methods in medical imaging and intelligent visual content generation that are applied in XR. It concludes also with possible developments and open challenges in AI application in Extended Reality-based solutions. Finally, the future lines of research and development directions of Artificial Intelligence applications both in medical image segmentation and Extended Reality-based medical solutions are discussed.

**Keywords:** Artificial Intelligence; Extended Reality; medical image scan segmentation.

## 1. Introduction

The human brain, a paramount example of evolutionary biological sophistication, transcends its anatomical categorization. Constituted by an estimated 86 billion neurons linked through an intricate web of synapses (ranging in the trillions), it is the epicenter of our cognitive, emotional, and consciousness-related functions [1]. This masterful structure of the central nervous system represents a nexus of myriad neurobiological processes, intricately overseeing sensory input conversion, motoric responses, and advanced cognitive functionalities. As a product of relentless evolutionary adaptations spanning millions of years, the brain epitomizes the apex of neurobiological optimization, synergizing complex neural circuitry with higher-order cognitive undertakings such as cognitive reasoning, emotional homeostasis, and the intricate processes of memory encoding, storage, and retrieval [1-3]. Thus, the human brain is a super-complex system whose functioning and intelligence depend rather on the type of neurons (depending on their role in the brain), their connections, and the way of supplying energy to neurons than the number of neurons [2]. It is an ideal reference model for the foundations of Artificial Intelligence (AI) [3,4].

Thus, processing and analysis of biomedical data for diagnostic purposes is a multidisciplinary field that combines AI, Machine Learning (ML), biostatistics, time series analysis as well as statistical physics and algebra (e.g. graph theory) [3]. Variables derived from biomedical phenomena can be described in several ways and in different domains (time, frequency, spectral values, spaces of states describing the biological system), depending on the characteristics and type of signal. Effective diagnosis of the early stages of the disease, as well as the determination of disease development trends, is a very difficult issue that requires taking into account many factors and parameters. Therefore, the state spaces of biomedical signals are huge and impossible to fully search, analyze, and classify even with the use of powerful computational resources. Therefore, it is necessary to use Artificial Intelligence, in particular, bio-inspired AI methods to limit research to a smaller but significant part of the state space.

Recently, computer-generated three-dimensional (3D) images have become increasingly important in medical diagnostics [5,6]. In particular, Extended Reality (XR) so-called Metaverse is increasingly used in health care and medical education, while it enables the deeper experience of the virtual world, especially through the development of depth perception, including the rendering of several modalities like vision, touch, and hearing [7]. In fact, medical images have different modalities and their accurate classification at the pixel level enables the accurate identification of disorders and abnormalities [8,7]. However, creating a 3D model of organs and/or their abnormalities is time-consuming and is often done manually or semi-automatically[10]. AI can automate this process and also contribute to increasing the quality of the resulting 3D objects [11,12] as well as visual content in the Metaverse [4,13]. To give the users a real sense of visual immersion, the developers should implement virtual objects of high quality [14]. In the context of medicine, it is combined with good quality medical data and their classification/segmentation algorithms with high accuracy, to faithfully reproduce the content in virtual three dimensions.

In this study, we aim to determine existing research gaps in the area of broadly understood medicine, including clinical trials in the application of explainable Artificial Intelligence. For that reason, this paper focuses on the overview of Artificial Intelligence-based algorithms in medical image scan segmentation and intelligent visual content generation in Extended Reality, including different types of neural networks used and learning rules, taking into account mathematical/theoretical foundations, algorithm accuracy, and performance, as well as open data availability. Specifically, we aim to answer the following research questions: can AI-

based algorithms be used for the accurate segmentation of medical data?, and how can AI-based algorithms be beneficial in Extended Reality-based technologies?

## 2. Materials and Methods

The methodology of the systematic review was based on the PRISMA Statement which was published in several journals [15] and its extensions: PRISMA-S [16]. We considered recent publications, reports, protocols, and review papers from Scopus and Web of Science databases. The keywords: Artificial Intelligence, Machine Learning, Extended Reality, Mixed Reality (MR), Virtual Reality (VR), Metaverse, learning algorithms, learning rules, signal classification, signal segmentation, medical image scan segmentation, segmentation algorithms, classification algorithms, and their variations. The selected sources were analyzed in terms of compliance with the analyzed topic, and then their contribution to medical image scan segmentation. First, the obtained title and abstract were independently evaluated by the authors. The duplicated records have been removed. Moreover, we have considered the inclusion of criteria-like publication in the form of journal papers, books, and proceedings as well as technical reports. The search was limited to full-text articles in English, including electronic publications before printing. Also, the exclusion criteria like Ph. D. thesis and materials not related to medical image scan segmentation and Artificial Intelligence-based algorithms have been adopted. Subsequently, articles meeting the criteria were retrieved and analyzed. The documents used in this study were selected based on the procedure presented in **Figure 1**. Finally, 162 documents were taken into account. The main limitation of the presented study was the fact that the field of medical image segmentation was lack of the theoretical principles in the considered paper, and lacked critical information concerning development algorithms based on Artificial Intelligence, such as type of the neural network, neuron model, information concerning details in data sets, input and output parameter, learning rules (treating AI-based systems) like a black box.

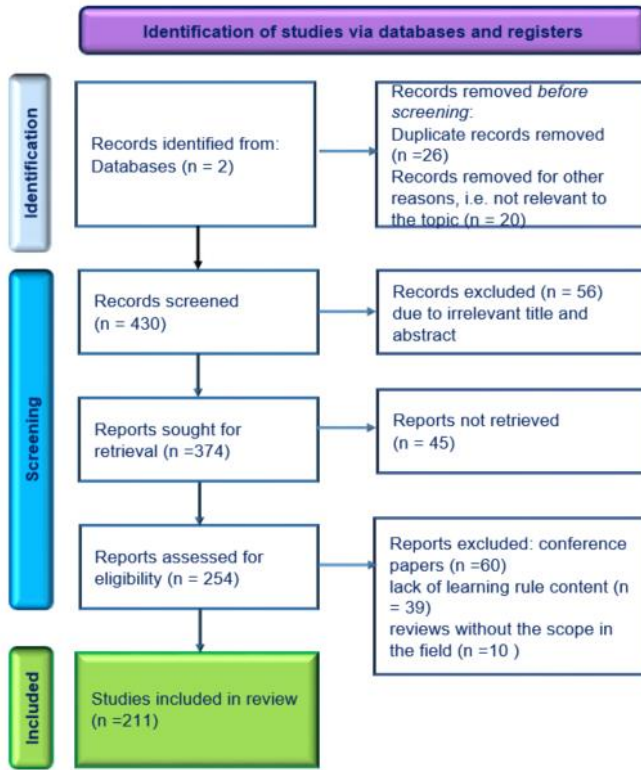


**Figure 1.** The scheme of the methodology of literature review.

In this study, we concentrate on the theoretical foundation of neural communication, the model of neurons, the type of neural networks, and learning rules with a special emphasis on their application in medical image scan segmentation and intelligent visual-content generation. We analyzed the Artificial Neural Networks (ANNs), Convolutional Neural Networks (CNNs), Recurrent Neural Networks (RNNs), Spiking Neural Networks (SNNs) as well as Generative Adversarial Networks (GAN), Graph Neural Networks (GNNs) and Transformers. The first one is made by the simplest neuron model (i.e. perceptions) and can process the information only in one direction. The second one consists of multilayer perceptrons and contains one or more convolutional layers that are responsible for the creation of feature maps, which are subjected to nonlinear processing. RNNs save the output to the processing nodes and feed the result back into the network (bidirectional information processing). The last type is closest to the real nervous system. SNNs transmit the information in the case the membrane potential of a neuron reaches the threshold not in every cycle of propagation like other listed neural networks. Another field that we analyzed in the context of medicine is learning rules, including backpropagation (i.e. in which the weight of the network is calculated according to the chain rule of the partial derivatives of the error function), ANN-SNN Conversion (i.e. transforming SNN networks into ANNs and application of the learning rules that are efficient in ANNs), Supervised Hebbian Learning (i.e. the postulate based on the rule that when the human brain in learning the neurons activates), Reinforcement Learning with Supervised Models (i.e. it enables the monitoring the reaction on the learning rule),

Chronotron (i.e. learning rules which take into account both, spiking neuron and the time of spiking), and biologically inspired network learning algorithms.

### 3. Neural communication

Neurons, which are basic brain building blocks, function as the core computational units of the brain, underpinning the vast expanse of conscious and subconscious processes, and defining our neural identity with each electrochemical interaction [11]. Neurons communicate with other neurons, and non-neuronal cells like muscles and glands by biological connections called “chemical synapses”, which are the communication points, at which sending nerve cells called presynaptic neurons, transmit the message to receiving nerve cells called the postsynaptic neuron. The presynaptic neuron releases neurotransmitters, a diverse group of chemicals, into the synaptic cleft (i.e. small gap at which neurons communicate). Following the release, these compounds traverse the synaptic gap, interacting with receptors on the postsynaptic membrane, eliciting a series of intracellular events, potentially leading to the generation of an action potential, a transient depolarizing event propagated along the neuronal membrane.

Since the famous experiments of Adrian [17, 177], it is assumed that in the nervous systems (including the brain), information is transmitted through weak electric currents (on the order of 100 (mV)), in particular employing action potentials (spikes) that are a transient, sudden (1-2 millisecond) change in the membrane potential of the cell/neuron associated with the transmission of information [18]. The stimulus for the creation of an action potential is a change in the electric potential in the cell's external environment. A wandering action potential is called a nerve impulse. In literature [19,20] it is assumed that the sequences of such action potentials, called spike-trains, play a key role in the transmission of information, and the times of appearance of these action potentials play a significant role. Mathematically, such time sequences can be and are modeled in particular after digitalization as trajectories (or their various variants) of certain stochastic processes (Bernoulli, Markov, Poisson, ...) [19,21-27].

### 4. Taxonomy of neural network applied in the medical image segmentation process

The Artificial Neural Networks (ANNs) are constructed with the perceptron neuron model [28] that is based on the binary decision rule. If the linearly weights  $w_i$  the sum of the input signals (input vector  $x_i$ ) exceeds the threshold  $t_{hr}$  neuron fires (i.e. the output is equal to 1) or if not output is equal to 0.

The basic input function is described as follows

$$f(x) = \begin{cases} 1, & \text{if } w_1x_1 + w_2x_2 + \dots + w_nx_n \geq t_{hr} \\ 0, & \text{otherwise} \end{cases} \quad (1)$$

The output vector of all neurons in  $l$ -th layer can be expressed as well as the combination of the linear transformation and non-linear mapping (i.e. ANN activation values) [29].

$$a^l = h(W^l a^{l-1}), i = 1, \dots, M \quad (2)$$

where  $W^l$  is the weight matrix between layer  $l$  and  $l - 1$ , and  $h(\cdot)$  denotes the activation function, in this case, Rectified Linear Unit (ReLU)  $f(x) = x^+ = \max(0, x)$  and the vector  $a^l$  denotes the output of all neurons in  $l$ -th layer. The formula (2) has been quoted following the designations in the publication [29]. Neuron models from the Integrate-and-Fire family are among the simplest, however, also the most frequently used. They are classified as spiking models. From a biophysical point of view, action potentials are the result of currents flowing through ion channels in the membrane of nerve cells. The Integrate-and-Fire neuron model [30, 31] focuses on the dynamics of these currents and the resulting changes in membrane potential. Therefore, despite numerous simplifications, these models can capture the essence of neuronal behavior in terms of dynamic systems.

The concept of Integrate-and-Fire neurons is the following: the input ion stream depolarizes the neuron's cell membrane, increasing its electrical potential. An increase in potential above a certain threshold value  $U_{thr}$  produces an action potential (i.e. an impulse in the form of Dirac's delta) and then the membrane potential is reset to the resting level. The leaky Integrate-and-Fire (LIF) neuron model [30, 31] is an extended model of the Integrate-and-Fire neuron, in which the issue of time-independent memory is solved by equipping the cell membrane with a so-called leak. This mechanism causes ions to diffuse in the direction of lowering the potential to the resting level or another level  $U_0 \rightarrow U_{leak} < U_{thr}$ . Thus, the third generation of neural networks, i.e. the Spiking Neural Networks (SNN) [32] are mostly based on the LIF, where the membrane potential  $U(t)$  is determined by the equation

$$\tau_m \frac{dU}{dt} = -[U(t) - U_{rest}] + R_m I(t) \quad (3)$$

where  $\tau_m$  is the membrane time constant of the neuron,  $R_m$  is total membrane resistance, and  $I(t)$  is the electric current passing through the electrode. The spiking events are not explicitly modeled in the LIF model. Instead, when the membrane potential  $U(t)$  reaches a certain threshold  $U_{th}$  (spiking threshold), it is instantaneously reset to a lower value  $U_{rest}$  (reset potential) and the leaky integration process starts a new one with the initial value  $U_r$ . To mention just a little bit of realism to the dynamics of the LIF model, it is possible to add an absolute refractory period  $\Delta_{abs}$  immediately after  $U(t)$  hits  $U_{th}$ . During the absolute refractory period,  $U(t)$  might be clamped to  $U_r$ , and the leaky integration process is re-initiated following a delay of  $\Delta_{abs}$  after the spike. More generally, the membrane potential (3) can be presented as

$$U(t) = \sum_{i=1}^N \omega_i \sum_{t_i < t} u(t - t_i) \quad (4)$$

where  $u(t)$  is a fixed causal temporal kernel that is an operation that allows scale covariance and scale invariance in a causal-temporal and recursive system over time [33] and  $\omega_i, i = 1, \dots, N$  denotes the strength of neuron synapses. Following Equation (2), the neuron's output  $m^l(t)$  (membrane potential after the neuron firing) can be described as follows [29]

$$m^l(t) = v^l(t-1) + W^l x^{l-1}(t) \quad l = 1, \dots, N \quad (5)$$

where  $v^l$  denotes the membrane potential before the neuron fires,  $W^l$  is the weight in  $l$ -th layer ( $l$  denoted layer index), and  $x^{l-1}(t)$  is the input from the last layer. Thus, to avoid the loss of information the “reset-by-subtraction” mechanism was introduced [34]

$$v^l(t) - v^l(t-1) = W^l x^{l-1}(t) - (H(m^l(t) - \theta^l) \theta^l) \quad (6)$$

where  $v^l(t)$  is membrane potential after firing,  $m^l(t)$  – membrane potential before firing,  $H(m^l(t) - \theta^l)$  refers to the output spikes of all neurons, and  $\theta^l$  is a vector of the firing threshold  $\theta^l$ . There are also some applications of the concepts of the meta-neuron model in SNNs [35]. The main differences between the LIF neuron and meta neurons stay in the integration process, where meta neurons use a 2nd-order ordinary differential equation and an additional hidden variable. The basic differences between ANN and SNN (taking into account the type of neuron models) are presented in **Figure 1**.

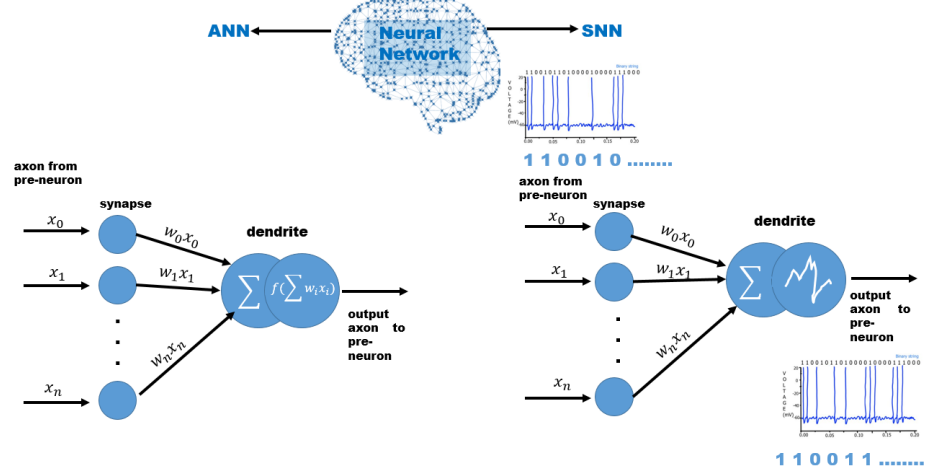


**Figure 2.** The scheme of the basic differences between ANN and SNN takes into account the type of neuron models.

#### 4.1. Convolutional Neural Network

The most commonly used deep neural network (DNN) in medical image classification is the two-dimensional (2D) Convolutional Neural Network (CNN) [36,37]. In **Figure 2**. The basic scheme of the SNN is presented. Its principle of operation is based on linear algebra, in particular matrix multiplication. CNNs consist of three types of layers: a convolutional layer, a pooling layer, and a fully connected layer. In fact, most computations are performed in the convolutional layer or layers. The image (pixels) is converted into binary values and patterns are searched. Every convolutional layer operates a dot product between two matrices, namely one matrix is a set of learnable parameters (kernel), and the second matrix is a limited part of the receptive field. Each subsequent layer contains a filter/kernel that allows you to classify features with greater efficiency. A pooling layer reduces the number of parameters in the input, which causes the loss of part of the information calculated in the common layer/layers, however, it allows for improvement in the efficiency of the CNN network. This operation is performed by sliding windows [38]. Next, the output of these two layers is transformed into a one-dimensional vector, i.e. input to the fully connected layer. In this last type of layer, image classification based on the features extracted in the previous layers is performed, i.e. the object in the image is recognized. The output  $y_{i,j}^{(k)}$  from CNN can be described as follows

$$y_{i,j}^{(k)} = \sigma(\sum_{l=1}^L \sum_{m=1}^M x_{i+l-1, j+m-1}^{(l)} w_{l,m}^{(k)} + b^{(k)}) \quad (7)$$

where  $x_{i,j}^{(l)}$  denotes input to the network at the spatial location  $(i,j)$ ,  $\sigma$  is the activation function,  $w_{l,m}^{(k)}$  is the weight of the  $m$ th kernel at the  $l$ th channel producing the  $k$ th feature map, and  $b^{(k)}$  is the bias for  $k$ th feature map.

In the case of large datasets, CNN achieves high efficiency and is resistant to noise [39]. The crucial disadvantages of CNNs in image processing are high computational requirements and difficulties in achieving high efficiency in the case of small datasets (i.e. if the dataset is too small the network may overfit to training data, and poorly recognize new data).

Input Layer  $\mathbf{X}$       Hidden Layer  $\mathbf{H}$       Output signal  $\mathbf{Z}$

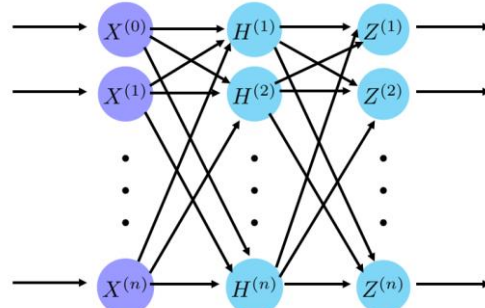


**Figure 3.** The basic scheme of the simple Convolutional Neural Network.

#### 4.2. Recurrent Neural Network

Another neural network commonly applied in medical data analysis is the Recurrent Neural Network (RNN) [40]. In the **Figure 3**. The basic scheme of the RNN is presented. This type of network contains at least one feedback connection. The output of RNN can be expressed as [41]

$$y_i = W_{hy} \mathcal{H}(W_{hh}h_{i-1} + W_{xh}x_i + b_h)h_i + b_y \quad (8)$$

where  $x_i, i = 1, \dots, T$  is the input sequence of  $T$  states  $(x_1, \dots, x_T)$  with  $x_i \in \mathbb{R}^d$ ,  $W_{xh}$ ,  $W_{hy}$ ,  $W_{hh}$  denotes weight matrices,  $b_h$ ,  $b_y$  are bias vectors, and  $\mathcal{H}$  is the non-linear activation function, for example, ReLU, Sigmoid  $f(x) = \frac{1}{1+e^{-x}}$ , Tanh Function (Hyperbolic Tangent)  $f(x) = \frac{e^x - e^{-x}}{e^x + e^{-x}}$ . The network operation is recursive since the hidden layer state depends on the current input and the previous state of the network. Thus, the hidden state  $h_{i-1}$  is the memory of past inputs.

Thus, the RNN can operate on the sequential dataset and has an internal memory. It may have many inputs. However, RNNs exhibit learning-related problems, namely vanishing gradients (i.e. in the case of small gradients the updates of parameters are irrelevant) or exploding gradients (i.e. superposition of large error gradients leading to large parameter updates). These contribute to the long training process, low level of accuracy, and low network performance.

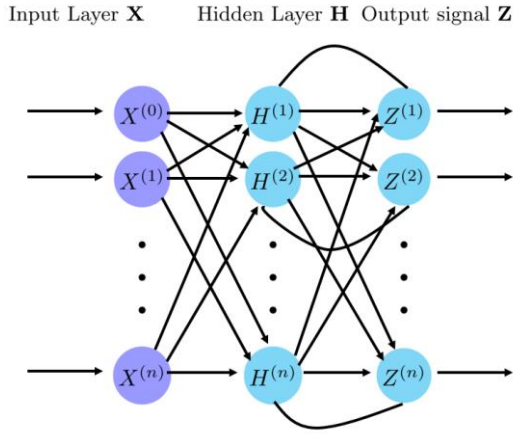


**Figure 3.** The basic scheme of the simple Recurrent Neural Network.

#### 4.3. Spiking Neural Networks

Besides the Artificial Neural Networks, i.e. CNNs, and RNNs, one can also be applied to the medical signals bio-inspired neural networks like Spiking Neural Networks [41,42]. In the **Figure 4**. The basic scheme of the SNN is presented. SNNs encode information taking into account spike signals, and shells are promising in effectuating more complicated tasks, while the more spatiotemporal information is encoded with spike patterns [43]. They are mostly based on the LIF neuron model. SNNs were formulated to map organic neurons, i.e. the appearance of the presynaptic spike at synapse triggers the input signal  $i(t)$  (the value of the current) that in the simplified cases can be written as follows

$$i(t) = \int_0^\infty S_j(s - t) \exp\left(\frac{-s}{\tau_s}\right) ds \quad (9)$$

where  $\tau_s$  denotes synaptic time constant,  $S_j$  is a presynaptic spike train,  $t$  is time [44]. In contrast, the majority of DNNs do not take into account temporal dynamics [45]. In fact, SNNs show promising capability in playing a similar performance as living brains. Moreover, the binary activation in SNNs enables the development of dedicated hardware for neuromorphic computing [46]. The potential benefits are low energy usage and greater parallelizability due to the local interactions.

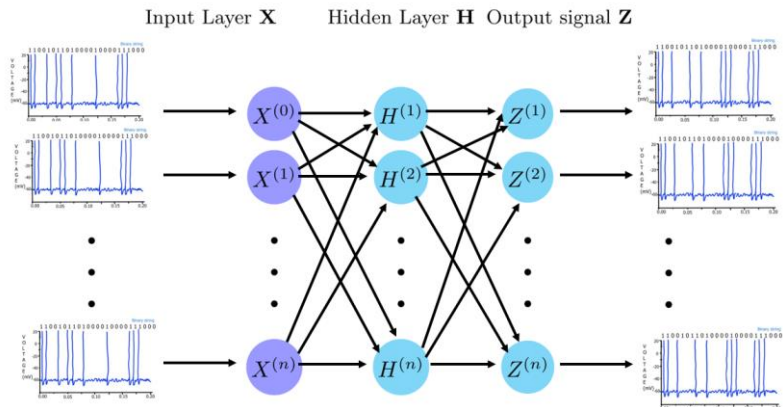


**Figure 4.** The basic scheme of the simple Spiking Neural Network.

#### 5. Learning algorithms

The heart of Artificial Intelligence is its learning algorithms. At their core, strive to automate the learning process, enabling machines to recognize patterns, make decisions, and predict outcomes based on data. Their design is often a balance between theoretical rigor and practical applicability. While mathematics and statistics provide the foundation, translating these into algorithms that can operate on vast and diverse datasets requires creative programming skills [22]. One can distinguish many types of network training algorithms [47]. Below we briefly discuss the most important of them, taking into account the theoretical foundations.

### 5.1 Back Propagation Algorithm

The most commonly used learning algorithm is the back propagation (BP) algorithm. It iterates over weight optimizations via error propagation in the neural networks. BP plays a pivotal role in enabling neural networks to recognize complex and non-linear patterns from large datasets [23, 48, 49]. From the mathematical point of view, it is a calculation of the cost function, which minimizes the calculated error of the output using gradient descent or delta rule [50]. It can be split into three stages: forward calculation, backward calculation, and computing the updated biases and weights. The input to the hidden layer  $H_j$  is the weighted sum of the outputs of the input neurons and can be described as [51]

$$H_j = b_{in} + \sum_{i=1}^n x_i w_{ij} \quad (10)$$

where  $x_i$  is the input to the network (input layer),  $n$  is the number of neurons in the input layer,  $b_{in}$  is the bias input layer, and  $w_{ij}$  denotes the weight associated with the  $i$ -th input neuron and the  $j$ -th hidden neuron. The output  $y_k$  is as follows

$$y_k = b_h + \sum_{j=1}^m w_{jk} F(H(j)) \quad (11)$$

where  $F(H(j))$  is a transfer function,  $k$  is the number of neurons in the hidden layer, and  $b_h$  is the bias of the hidden layer. The most commonly used transfer function is the sigmoid transfer function  $F(H(j)) = \frac{1}{1+e^{-(H(j))}}$ . The back propagation algorithm is especially effective when used in multi-layered neural architectures such as feed-forward neural networks, convolutional neural networks, and recurrent neural networks [26]. In image recognition, CNNs, energized by BP, can independently identify hierarchical features, from basic edges to detailed structures. Similarly, RNNs, amplified by BP, are adept at sequence-driven tasks like machine translation or speech recognition, as they incorporate previous data to influence present outputs. It is one of the most effective deep learning methods. However, BP requires large amounts of data and enormous computational efforts.

### 5.2 ANN-SNN Conversion

Artificial Neural Networks and Spiking Neural Networks are both computational models inspired by biological neural networks. While ANNs have been the mainstream for most deep learning applications due to their simplicity and effectiveness, SNNs are gaining traction because they mimic the behavior of real neurons more closely by using spikes or binary events for communication. To obtain a similar accuracy of the SNN-based algorithm as the algorithm using ANN, for example, the BP-type training rule consumes a lot of hardware resources. The already existing platforms have limited optimization possibilities. Thus, the conversion of ANNs to SNNs seeks to harness the energy efficiency and bio-realism of SNNs without reinventing the training methodologies [28], while it is based on the ReLU activation function and LIF neuron model [52]. The basic principle of the conversion of ANNs to SNNs is mapping the activation value of the ANN neuron to the average postsynaptic potential (in fact, firing Rate) of SNN neurons, and the change of the membrane potential (i.e. the basic function of spiking neurons) can be expressed by the combination of the Equation (2) and Equation (6)[29]

$$v^l(t) - v^l(t-1) = W^l x^{l-1}(t) - s^l(t) \theta^l \quad (12)$$

Here  $s^l(t)$  refers to the output spikes of all neurons in layer  $l$  at time  $t$ .

Tuning the right thresholds is paramount for the SNN to effectively and accurately represent information. Incorrectly set thresholds could lead to either too frequent or too rare spiking, potentially affecting the accuracy of the SNN post-conversion [35]. On the other hand, the neuromorphic hardware platforms that support SNNs natively can primarily offer energy efficiency benefits by converting ANNs to SNNs. Due to their event-driven nature, SNNs can be more computationally efficient [36]. However, the challenge lies in maintaining accuracy post-conversion. Some information might be lost during the transition, and not all ANN architectures and layers neatly convert to their SNN equivalents. The conversion from ANNs to SNNs is a promising direction, merging the advanced training methodologies of ANNs with the energy efficiency of SNNs. As we delve deeper into the realm of neuromorphic computing, this conversion process will play a pivotal role in bridging traditional deep learning with biologically-inspired neural models [37, 38].

### 5.3 Supervised Hebbian Learning (SHL)

Taking into account Artificial Intelligence, Supervised Hebbian Learning (SHL) can be described as a general methodology for weight changes [53]. Thus, this weight increases when two neurons fire at the same time, while it decreases when two neurons fire independently. According to this rule, the change in weight can be written

$$\Delta w = \eta(t^{out} - t^d) \quad (13)$$

where  $\eta$  is the learning rate (in fact, the small scalar that may vary with time,  $\eta > 0$ ),  $t^{out}$  the actual time of the postsynaptic spike, while  $t^d$  is the time of firing of the second presynaptic spike [54, 55]. The crucial disadvantage of Hebbian learning is the fact that when the number of hidden layers increases the efficiency decreases, while in the case of 4 layers is still competitive [56].

### 5.4 Reinforcement Learning with Supervised Models

According to the additional constraints in the SHL rule, Reinforcement Learning with Supervised Models (ReSuMe) was proposed [54]. ReSuMe, is a dynamic hybrid learning paradigm. It effectively combines the resilience of Reinforcement Learning

(RL) with the precision of Supervised Learning (SL). This fusion empowers ReSuMe to leverage feedback-driven mechanisms inherent in RL and take advantage of labeled guidance typical for SL [37,38, 39]. The difference between SHL is that the learning signal is expected not to have or have a marginal direct effect on the value of the postsynaptic somatic membrane potential [57], thus the synaptic weights are modified as follows

$$\frac{d}{dt} \mathbf{w}_{ji}(\mathbf{t}) = \mathbf{a}[\mathbf{S}_d(\mathbf{t}) - \mathbf{S}_j(\mathbf{t})]\bar{\mathbf{S}}_i(\mathbf{t}) \quad (14)$$

where  $\mathbf{a}$  denoted learning rate,  $\mathbf{S}_d$  is desired/targeted spike train,  $\mathbf{S}_j(\mathbf{t})$  is the output of the network (spike train), and  $\bar{\mathbf{S}}_i(\mathbf{t})$  expresses the low-pass filtered input spike train. ReSuMe guided one of its most salient features exploration. By leveraging labeled data *via* SL, ReSuMe can effectively steer RL exploration, ensuring agents avoid falling into the trap of suboptimal policies. The hybrid nature of ReSuMe also grants it a unique resilience, especially in the face of noisy data or in reward-scarce environments. Moreover, its adaptability is noteworthy, making it an ideal choice for tasks that combine immediate feedback (through SL) with long-term strategic maneuvers (through RL). However, like all things, ReSuMe is not without challenges. A potential bottleneck in ReSuMe is computational complexity, as managing both RL and SL can sometimes strain computational resources. Another challenge is the precise tuning of the  $\mathbf{a}$  coefficient. The key is to find a balance where neither RL nor SL overly dominates the learning process. By melding immediate feedback from supervised learning with a deep reinforcement learning strategy, ReSuMe establishes itself as a formidable tool in Machine Learning [49, 50, 52].

## 5.5 Chronotron

The Chronotron, by its essence, challenges and reshapes our understanding of how information can be encoded and processed in neural structures [50, 55]. Traditional neural models have predominantly focused on the spatial domain, emphasizing the architecture and interconnections between neurons. While this spatial component is undeniably critical, it offers only a part of the full informational symphony that the brain plays. Just as the rhythm and cadence of a song contribute as much to its essence as its melody, in the vast theater of the brain, timing is not just a factor; it is a storyteller in its own right. The brilliance of the Chronotron lies in its ability to discern and respond to this temporal narrative. Unlike its counterparts, which often treat time as a secondary parameter, the Chronotron places it center stage. As a consequence, it acknowledges and leverages the intricate interplay of spatial and temporal dynamics in neural computation. This means that it doesn't just consider which neurons are firing, but also pays meticulous attention to when they fire concerning one another. Thus, the membrane potential is

$$\mathbf{u}(\mathbf{t}) = \boldsymbol{\eta}(\mathbf{t}) + \sum_j \mathbf{w}_j \sum_{t_j^f \leq t} \boldsymbol{\varepsilon}_j(\mathbf{t}, t_j^f) \quad (15)$$

where the models the  $\boldsymbol{\eta}$  model's refractoriness is caused by the past presynaptic spikes,  $\mathbf{w}_j$  is the synaptic efficacy,  $t_j^f$  is the time of appearance of the  $f$ -th presynaptic spike on the  $j$  synapse,  $\boldsymbol{\varepsilon}_j(\mathbf{t}, t_j^f)$  denotes normalized kernel [58]. When  $\mathbf{u}(\mathbf{t})$  reaches the threshold level, a spike is fired. And  $\mathbf{u}(\mathbf{t})$  is reset to the value of reset potential. In this approach, it is crucial to find the appropriate error functions, i.e. such an error function that enables the minimization with a gradient descent method [59]. The advantage of this learning rule is the fact that it uses the same coding for inputs and outputs. Chronotron's hallmark, its granularity, can sometimes surge computational demands, especially during intense training. And like many cutting-edge neural frameworks, harnessing Chronotron's full potential can be intricate, necessitating fine-tuned parameters and rich, well-timed data.

## 5.6 Bio-inspired Learning Algorithms

Brain-inspired Artificial Intelligence approaches, in particular spiking neural networks, are becoming a promising energy-efficient alternative to traditional artificial neural networks [60]. However, the performance gap between SNNs and ANNs has been a significant obstacle to the wild SNNs application (applicable SNNs). To fully use the potential of SNNs, including the detection of the non-regularities in biomedical signals, and designing more specific networks, the mechanisms of their training should be improved, one of the possible directions of development is the bio-inspiring learning algorithms. Below we briefly discuss the most important of them.

### 5.6.1 Spike Timing Dependent Plasticity

Spike Timing Dependent Plasticity (STDP) is rooted in the idea that the precise timing of neural spikes critically affects changes in synaptic strength [61]. This principle highlights the intricate dance between time and neural activity, showcasing the dynamics of our neural circuits. This biologically plausible learning rule is a timing-dependent specialization of Hebbian learning (13) [62]. STDP shed light on the intricate interplay between timing and synaptic modification. It is based on the change in synaptic weight function

$$\Delta \mathbf{W} = \boldsymbol{\eta}(1 + \zeta) \mathbf{H}(\mathbf{W}; \mathbf{t}_{pre} - \mathbf{t}_{post}) \quad (16)$$

where  $\boldsymbol{\eta}$  denotes the learning speed,  $\zeta$  is Gaussian white noise with zero mean, while  $\mathbf{H}(\mathbf{W}; \mathbf{t}_{pre} - \mathbf{t}_{post})$  is the function, that determines the long-term potentiation (LTP, i.e. presynaptic and postsynaptic neurons emit a high rate) and depression (LTD, i.e. presynaptic neurons emit a high rate) in the time window  $\mathbf{t}_{pre} - \mathbf{t}_{post}$  [63]

$$\mathbf{H}(\mathbf{W}; \mathbf{t}_{pre} - \mathbf{t}_{post}) \begin{cases} \mathbf{a}_+(\mathbf{W}) \exp(-\frac{|\mathbf{t}_{pre} - \mathbf{t}_{post}|}{\tau_+}) & \text{for } \mathbf{t}_{pre} - \mathbf{t}_{post} < 0 \\ -\mathbf{a}_-(\mathbf{W}) \exp(-\frac{|\mathbf{t}_{pre} - \mathbf{t}_{post}|}{\tau_-}) & \text{for } \mathbf{t}_{pre} - \mathbf{t}_{post} > 0 \end{cases} \quad (17)$$

where  $a(W)$  is a scaling function that determines the weight dependence, while  $\tau$  denotes the time constant for depression [61-63]. STDP's significance is underpinned by its numerous advantages. Chiefly, it offers a biologically authentic model by 'mimicking the temporal dynamics observed in real neural systems. Furthermore, its event-centric nature promotes unsupervised learning, enabling networks to autonomously adjust based on the temporal patterns present in input data. This time-based sensitivity equips STDP to adeptly process data with spatiotemporal attributes and detect intricate temporal relationships within neuronal signals [64, 65]. However, STDP is not without its complexities. A prominent challenge is the fine-tuning of parameters. The exact values assigned to constants like  $a(w)$  and  $\tau$  can substantially dictate the behavior and efficacy of STDP-informed networks. Balancing these values requires a meticulous approach. Moreover, the precision demanded by STDP's time-centric nature often calls for higher computational rigor, especially within simulation contexts. STDP stands as a testament to the elegance and intricacy of neural systems. By emphasizing the role of spike timing, STDP offers a vivid depiction of how synaptic interactions evolve [66, 67].

### 5.6.2 Spike-Driven Synaptic Plasticity

Spike-Driven Synaptic Plasticity (SDSP) offers the ability to elucidate the causality in neural communication. It operates on a fundamental principle: the sequence and timing of spikes determine whether a synapse strengthens or weakens. If a neuron consistently fires just before its downstream counterpart, it's a strong indication of its influential role in the latter's activity. This "pre-before-post" firing often leads to synaptic strengthening, cementing the relationship between the two neurons. Conversely, if the sequence is reversed, with the downstream neuron firing before its predecessor, the connection may weaken, reflecting a lack of causal influence [68, 69]. This causative aspect of SDSP provides valuable insights into the learning mechanisms of the brain. It suggests that our neural circuits are continually evolving, adjusting their connections based on the flow of spike-based information. Such adaptability ensures that our brains remain receptive to new information, enabling us to learn and adjust to ever-changing environments. Moreover, SDSP emphasizes the significance of precise spike timing. In the realm of neural computation, milliseconds matter. Small shifts in spike timing can change a synapse's fate, showcasing the brain's precision and sensitivity. This meticulousness in spike-driven modifications underscores the importance of timing in neural computations, hinting at the brain's capacity to encode and process temporal patterns with remarkable accuracy [70-73]. In this learning rule the changes in synaptic weights can be expressed as [64]

$$\Delta w = \begin{cases} \eta^+ + e^{-|\Delta t|/\tau^+} & \text{if } \Delta t > 0 \\ \eta^- + e^{-|\Delta t|/\tau^-} & \text{otherwise} \end{cases} \quad (18)$$

where  $\eta_+ > 0$  and  $\eta_- < 0$  denotes the learning parameters,  $\tau_+$  and  $\tau_-$  are time constraints, and  $\Delta t$  is the difference between post- and pre-synaptic spikes. This representation, while streamlined, encapsulates the principle that the mere presence of a spike can induce modifications in the synaptic weight, either strengthening or weakening the connection based on the specific neural context and the directionality of the spike's influence [70].

The appeal of Spkipe-Driven Synaptic Plasticity is manifold its primary virtue is its biological relevance. Focusing on individual spike occurrences mirrors the granular events that take place in real neural systems. Such an approach facilitates the modeling of neural networks in scenarios where individual spike occurrences are of paramount importance. Furthermore, by anchoring plasticity on singular events, this model is inherently suitable for real-time learning and rapid adaptability in dynamic environments [Błąd! Nie można odnaleźć źródła odwołania.].

A crucial challenge lies in the accurate capture and interpretation of individual spikes, especially in densely firing neural environments. Moreover, the plasticity model's sensitivity to 'single events' means that it can be susceptible to noise, requiring sophisticated filtering mechanisms to discern genuine learning events from spurious spikes. SDS elucidates the profound influence of singular neuronal events on the grand tapestry of neural learning and adaptation [75].

### 5.6.3 Tempotron Learning Rule

One of the most interesting biological-inspired learning algorithms is the tempotron principle [65, 76, 77]. It is designed to adapt synaptic weights based on the temporal precise patterns of incoming spikes, rather than only the frequency of such spikes. While traditional neural models might emphasize synaptic weights or connection topologies, tempotron underscores that the 'when' of a neural event can be as informative, if not more so, than the 'where' or 'how often' [78-80]. The tempotron learning rule is based on the LIF neuron model. It fires when the membrane potential described by Equation (4) exceeds the threshold (binary decision). Thus, one can define the potential of the neuron's membrane as a weighted sum of postsynaptic potentials (PSPs) from all appearance spikes [77]

$$v(t) = \sum_i \omega_i \sum_{t_i} K(t - t_i) + V_{rest} \quad (19)$$

where  $\omega_i$  denotes synaptic efficacy,  $t_i$  is the firing time of the  $i$ th afferents,  $V_{rest}$  is resting potential, and  $K$  is the normalized PSP kernel

$$K(t - t_i) = V_0 \left( \exp\left(\frac{-(t-t_i)}{\tau_m}\right) - \exp\left(\frac{-(t-t_i)}{\tau_s}\right) \right) \quad (20)$$

where  $\tau_m$  is the decay time constant of membrane integration, while  $\tau_s$  denotes the decay time constant of synaptic currents. While the  $V_0$  normalized the PSP that the maximum kernel value is equal to 1. The neuron is fired when the value of the potential of the neuron's membrane described by Equation (19) is greater than the value of the firing threshold. Next, the potential of the neuron's membrane described by Equation (19) smoothly decreases to the value of  $V_{rest}$ . In the case of the segmentation/classification task, the input to the neuron may belong to one of two classes, namely  $P^+$  when a stimulus occurs (i.e. pattern is presented) the neuron

should fire), and  $\mathbf{P}^-$  when the pattern is presented neuron should not fire. Each input consists of  $N$  spike trains. In turn, the tempotron learning rules are as follows

$$\Delta\omega_i = \lambda \sum_{t_i < t_{max}} K(t_{max} - t_i) \quad (21)$$

where  $t_{max}$  is the time when the potential of the neuron's membrane (19) reaches a maximum value. While  $\lambda$  is the constant that is greater than zero in the case of  $\mathbf{P}^+$ , and smaller than zero in the case  $\mathbf{P}^-$ . In this operation, tempotron introduces gradient-decent dynamics, i.e. minimizing the cost function for each input pattern measures the maximum voltage that is generated by the erroneous patterns. In comparison to the STDP learning rule, tempotron can make the appropriate decision under a supervisory signal, by tuning fewer parameters than STDP. Thus, tempotron uses LTP and LTD mechanisms like STDP. The advantage of the tempotron learning rule is the speed of learning.

## 6. Neural networks and learning algorithms in the medical image segmentation process

Image segmentation has a crucial role in creating both, medical diagnosing supported by image analysis and virtual object creation like the medical digital twin (DT) of organs [66,67], holograms of the human organs [81, 82], and virtual medical simulators [68, 83]. One can split the image segmentation process into semantic segmentation (i.e. assigning a label or category to each pixel), instance segmentation (i.e. identifying and separating individual objects in an image and assigning a label to it), and panoptic segmentation (i.e. more complex tasks, which involves the two segmentations above) [77, 78]. The application of AI enables to increase in the efficiency and speed of these processes [84]. In Table 1. the comparison of the AI-based algorithms applied in medical image scan segmentation taking into account the neuron model, the type of neural network, learning rule, and biological plausibility is shown. It turned out that the most commonly used in image segmentation are CNNs, in particular, Unet architecture and its variations [71,72, 74, 75, 85]. In [73] the authors modified this neural network structure by adding dense and nested skip connections (UNet++), while [178] added the residual blocks and attention modules to enable the network to learn deeper features and increase the effectiveness of segmentation. To connect the efficiency of segmentation with access to global semantic information, often CNNs are combined with transformer blocks [85-87]. Another CNNs-based algorithm commonly used in medical image segmentation is You Only Look Once (YOLO), which is open-source software used under the GNU General Public License v3.0 license [88, 179]. It uses one fully connected layer, the number (depending on the version) of convolution layers that are pre-trained with the CNN (YOLO v1 ImageNet, YOLO v2 Darknet-19, YOLO v3 Darknet-53, YOLO v4 CSPNet, YOLO v5 EfficientNet, YOLO v6 EfficientNet-L2, YOLO v7 ResNET, YOLO v8 RestNet), and pooling layer. The algorithm divides the input in the form of a photo into specific segmentations and then uses CNN to generate bounding boxes and class predictions. Recently, in image classification, SNN has become more popular [78, 79] due to its low power consumption. However, SNN training rules require refinement to achieve ANN accuracy. However, the development of an efficient, automatic segmentation procedure is of high importance [207].

Recently, Transformer Networks that were designed to machine translation (Natural Language Processing task) have been applied in the field of image processing, including medical image processing [180]. This architecture is based on network normalization feed-forward network and residual structures (namely Multi-Head Attention (MHA) and Positionwise Feed-Forward Networks), while it does not contain any convolutions [181]. Such an architecture enables them to achieve a powerful ability to represent long-term receivables. Thus, the architecture of transformers in the field of computer vision contains only vision transformers (ViT) and Swin transformers [182, 183]. The MHA has multiple attention modules which learn different aspects in different subspaces. In [184] was shown that Transformers may have a higher level of efficiency in the field of image processing compared to the CNNs taking into account learning which is applied to large datasets. To increase the applicability and accuracy of transformers in the area of image processing, data augmentation and regularization strategies are used, among others [185]. On the other hand, vision transforms do not contain inductive biases. Also, the combination of CNNs and Transformers was applied to image processing [186], which contributed to reducing the consumption of computing resources and training time [187, 188]. The main disadvantages of Transformers are the need for commitment of large amounts of computational resources and the requirements of the long training time.

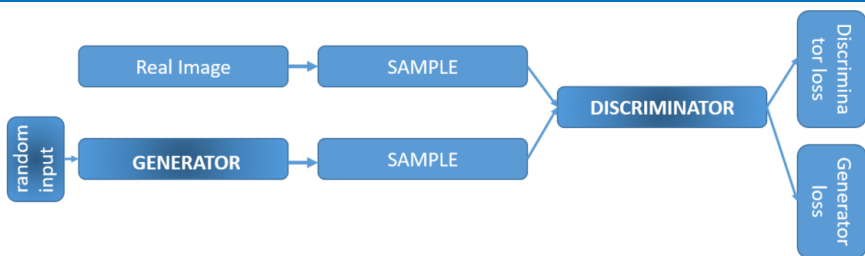


**Figure 5.** The basic scheme of the simple Generative Adversarial Network.

Also, Generative Adversarial Networks are applied to medical image fusion [190]. This type of approach divided the neural networks into two parts: generators (learn to generate reliable data. The generated instances become negative examples for training the second part of the network) and discriminators (i.e. binary classifiers that learn to distinguish generators from real data, see Figure 5. The discriminator presents a penalty for generating meaningful results. The output of the generator is connected directly to the input of the discriminator. In back-propagation, the discrimination classification determines the signal that the generator uses to update the weights. In fact, GANs are the paris of CNNs that are connected adversarial. The difference between them is their approach to getting results. For example, in [191, 192] GAN was successively applied to the segmentation of the blood vessels of

the retinal and the coronary with high accuracy. However, centralized training algorithms can potentially mishandle sensitive information such as medical data. Additionally, GANs have significant security issues, such as vulnerabilities that exploit the real-time nature of the learning process to generate prototype samples of private training sets [194]. Also, the use of deep neural networks such as CNN and GAN is limited by the need to have large annotated data sets, which is quite a challenge, especially in medicine [193].

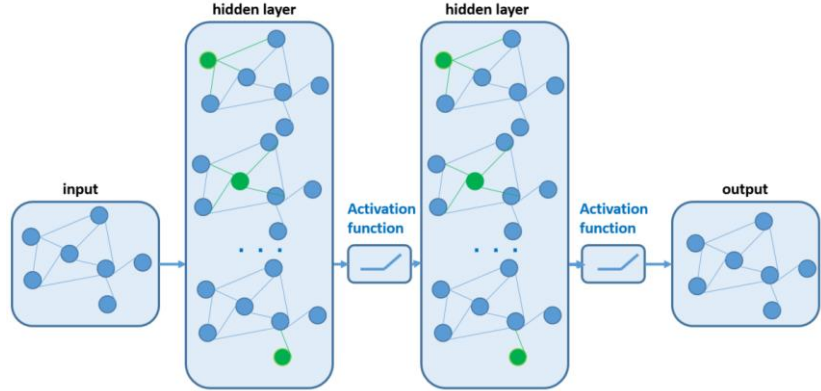


**Figure 6.** The basic scheme of the simple Graph Neural Network.

All the above solutions are based on Euclidean space data that have fixed dimensions. However, data can be also presented in non-Euclidean space (i.e. graphs, namely a set of objects (vertices) and relationships between these objects (edges)) [195]. This kind of data has dynamical dimensions, i.e. the input data do not have to be in particular order like in the case of Euclidean space data [196]. Thus, in the field of medical data processing also occur irregular spatial patterns that may be important for the diagnostics point of view. The analysis of these patterns is a challenge that is proposed to be solved by applying Graph Neural Networks [197, 202, 204]. GNNs are based on the convolution operation on the graphs, see Figure 6. One disadvantage of GNNs is the fact that they are strongly dependent on the geometry of the graph. Consequently, the neural network must be trained every time data is added. In the context of large image diagnostics, this can make a less practical approach. Also, the low computational speed of GNNs taking into account medical data processing contributes to the fact that GNNs need further development for practice applications. As a solution to improved calculation efficiency, a framework for inductive representation learning on large graphs i.e., GraphSAGE was proposed [198]. Thus, GNNs can expand the possibilities of training CNNs on non-grid data [199]. In the field of medical image segmentation, GNNs find especially application in tissue semantic segmentation in histopathology images [203, 205, 206]. In the case of tumor segmentation, the application of CNN leads to the number of parameters that contribute to the high computational complexity. Here, the combination of CNN and GNN is a very promising solution, like in the [206]. First, the two-layer CNN was applied to the creation of the feature maps, and then two GNN layers were used to selectively filter out the discriminative features.

Recently, also Sinusoidal Representation Networks so-called SIRENs were applied to image segmentation. The essence of this approach is based on periodic activation functions for implicit neural representations. In fact, this AI solution mostly applied the sine periodic activation function. In [208] was proposed to analyze images, and in [209, 210] to segment medical images (cardiac MRI). However, this approach in the field of medical image segmentation requires still improvement.

Another interesting algorithm for natural image segmentation with was recently developed (April 2023) by Meta is the Segmentation Anything Model (SAM) [89, 90]. This AI-based algorithm enables cutting out any object from the image with a single click. It uses CNNs and transformer-based architectures for image processing, in particular, transformers-based architectures are applied to extract the features, compute the embedding, and pump the encoder. The first attempt has been made to apply it in the field of medical imaging, however, in medical segmentation, it is still not so accurate in comparison to other application fields [91, 92]. The imperfections of the SAM algorithm in the field of medical image segmentation are mainly connected to insufficient numbers of training data. In [93], the authors proposed to apply the Med SAM Adapter to overcome the above limitations. The pre-training method like Masked Autoencoder (MAE), Contrastive Embedding-Mixup (e-Mix), and Shuffled Embedding Prediction (ShED) was applied. There is a lot of work in the area of medical image segmentation using machine learning, but relatively little addresses the issue related to the network learning process itself (along with data, a key element in achieving high accuracy of the process) [94].

The comparative comparison of the neural network architectures, learning algorithms, and datasets that are applied in the field of image segmentation in medicine is shown in **Table 1**. It turned out that still the most commonly used (taking into account accuracy of prediction) in these areas are ANN, and CNN constructed with the perceptrons and LIF neuron models and BP learning rules. Thus, the most commonly used learning algorithms in medical image segmentation are still on the low level of biological plausibility. On the other hand, in other image segmentation, in particular, biologically plausible learning algorithms are applied, for example, in the field of the images of handwritten digits [77]. Thus, **Table 1** presents works that contain information about the neuron model, architecture and type of neural network, input and output parameters to the network, and type of learning algorithm.

**Table 1.** The comparison of the AI-based algorithms applied in medical image scan segmentation

Net-work Type	Neuron model	Average Accuracy [%]	Data sets - training/testing/validation sets [%] or training/testing sets [%]	Input parameters	Learning rule	Biologi-cal plau-sibility	Ref.
---------------	--------------	----------------------	---	------------------	---------------	---------------------------	------

ANN	Perceptron	99.10	mammography images <i>lack of information</i>	mammography images – 33 features extracted by Region of Interest (ROI)	BP	low	[95]
CNN	Perceptron	98.70	Brain tumor, MRI color images 70/15/15	MRI image scan, 12 features (mean, standard deviation (SD), entropy, Energy, contrast, homogeneity, correlation, variance, covariance, root mean square (RMS), skewness, kurtosis)	BP	low	[96]
CNN	Perceptron	96.00	Echocardiograms 60/40	Disease classification, cardiac chamber segmentation, viewpoints classification in echocardiograms	<i>lack of information</i>	low	[97]
CNN	Perceptron	94.58	brain tumor images 50/25/25	brain tumor images	<i>lack of information</i>	low	[98]
CNN	Perceptron	91.10	simultaneous IVUS and OCT images	IVUS and OCT images	<i>lack of information</i>	low	[99]
CNN	Perceptron	98.00	2-D ultrasound 49/49/2	Classification of the cardiac view into 7 classes	<i>lack of information</i>	low	[100]
CNN	Perceptron	93.30	coronary cross-sectional images 80/20	Detection of motion artifacts in coronary CCTA, classification of coronary cross-sectional images	<i>lack of information</i>	low	[101]
CNN	Perceptron	99.00	MRI image scan 60/40	Bounding box localization of LV in short-axis MRI slices	<i>lack of information</i>	low	[102]
CNN and doc2vec	Perceptron	96.00	continuous wave Doppler cardiac valve images 94/4/2	Automatic generation of text for continuous wave Doppler cardiac valve images	<i>lack of information</i>	low	[103]
Deep CNN + complex data preparation	Perceptron	97.00	Vessel segmentation <i>lack of information</i>	proposing a supervised segmentation technique that uses a deep neural network. Using structured prediction	<i>lack of information</i>	low	[104]
CNN and Transformer encoders	Perceptron	90.70	Automated Cardiac Diagnosis Challenge (ACDC), CT image scans from Synapse 60/40	CT image scans	BP	low	[105]
CNN and Transformer encoders	Multi-layer Perceptron	77.48 (Dice coefficient)	Multi-organ segmentation <i>lack of information</i>	CT image scans - Synapse multi-organ segmentation dataset	BP	low	[189]
CNN and Transformer encoders	Perception	78.41 (Dice coefficient)	Multi-organ segmentation <i>lack of information</i>	CT image scans	BP	low	[181]
CNN, and RNN	Perceptron	95.24 (REs-Net50) 97.18(InceptionV3) 98.03 (Dense-Net)	MRI image scan of the brain 80/20	MRI image scan of the brain, modality, mask images	BP	low	[106]

<b>CNN, and RNN</b>	Perceptron	95.74 (REs-Net50) 97.14(Dark-Net-53)	skin image <i>lack of information</i>	skin image	BP	low	[107]
<b>SNN</b>	LIF	81.95	baseline T1-weighted whole brain MRI image scan <i>lack of information</i>	The hippocampus section of the MRI image scan	ANN-SNN conversion	low	[108]
<b>SNN</b>	LIF	92.89	burn images <i>lack of information</i>	256 × 256 burn image encoded into 24 × 256 × 256 feature maps	BP	low	[109]
<b>SNN</b>	LIF	89.57	skin images (melanoma and non-melanoma) <i>lack of information</i>	skin images converted into spikes using Poisson distribution	surrogated gradient descent	low	[110]
<b>SNN</b>	LIF	99.60	MRI scan of brain tumors 80/10/10	2D MRI scan of brain tumors	YO-LO-2-based transfer learning	low	[111]
<b>SNN</b>	LIF	95.17	microscopic images of breast tumor <i>lack of information</i>	microscopic images of breast tumor	Spike-Prop	low	[112]
<b>GAN</b>	Perceptron	83.70 (Dice coefficient) DRIVE dataset 82.70 (Dice coefficient) STARE dataset	segmentation of retinal vessels <i>lack of information</i>	dataset for retinal vessel segmentation: DRIVE dataset and STARE dataset	BP	low	[191]
<b>GAN</b>	Perceptron	94.60	segmentation of the blood vessels of the retinal and the coronary and for the knee cartilage <i>lack of information</i>	dataset for retinal vessel segmentation: DRIVE dataset and coronary dataset	BP	low	[193]
<b>GAN</b>	Perceptron	90.71 (Dice coefficient)	Brain segmentation data brain-MRI dataset 80/20	Brain MRI image scan	BP	low	[192]

**Legend:**

BP – back propagation,

ANN – Artificial Neural Network,

SNN – Spiking Neural Network,

YOLO – you only look once algorithm,

spike-prop – supervised learning rule akin to traditional error-back-propagation for a network of spiking neurons with reasonable post-synaptic potentials,

MRI – Magnetic resonance imaging,

OCT – optical coherence tomography,

IVUS – intravascular ultrasound,

CCTA – Coronary Computed Tomography Angiography,

LV – left ventricle,

CT – computer tomography,

T1 weighted image – the basic pulse sequences in MRI, it shows the differences in the T1 relaxation times of tissue (T1 relaxation measures of how quickly the net magnetization vector recovers to its ground state),

GAN – Generative Adversarial Networks.

The segmented structures (in this case organs and their disorders) may be next applied to the development of the 3D virtual environment [105]. These 3D objects may be implemented through for example, holograms displayed in the head-mounted display (HMDs) like Mixed Reality glasses in medical diagnostics [113], pre-operative imaging [114], surgical assistance [115, 116], robotics surgery [117], and medical education [81, 82]. However, the crucial issue is connected with the quality of obtained segmented structures, and this process can be significantly accelerated and improved by the use of Artificial Intelligence.

The crucial issue when the AI-based system is developed is connected with the accuracy and performance of algorithms. Many metrics have been introduced in image segmentation that enable the evaluation of algorithms. They can be split into two metric types, binary which takes into account two types of classification, and multi-class classification, in which the number of classes is higher than two. These metrics have been widely described in [163, 164]. The most commonly used metrics in medical image segmentation are the binary classifier *F-Score* (F-measure) or so-called *F1-Score* (also called Dice Coefficient) [165], Mean Absolute Error (*MAE*) [166], Mean Squared Error (*MSE*), Root-Mean-Squared Error (*RMSE*), Area Under Receiver Operator Curve (*AUROC*) [167] as well as Index of Union (*IoU*) [168].

## 7. Data availability

One of the key issues in the development of AI algorithms in the field of medicine is the availability and quality of data, i.e. access to electronic health records (EHRs) [118, 119]. Thus, the medical data should be anonymized. In **Table 2** a summary of publicly available retrospective image scan medical databases is presented. Some authors also provide anonymized data upon request. It is worth stressing that data, including medical image scans, are subjected to various types of biases [120]. The databases listed in Table 2 do not contain precise information regarding, for example, the ethnic composition of the study participants. Their age ranges and gender are usually disclosed. Moreover, another important issue concerning medical data is connected with Internet segmentation errors as was pointed out in the [169]. The authors discovered that the publicly available dataset contains duplicate records, which may contribute to the overlearning of some patterns in AI and ML models as well as result in false predictions. Also, the random procedure of splitting the database into training and testing sets will then influence the results obtained. As a consequence may lead to obtaining inflated classification.

**Table 2.** A summary of publicly available retrospective image scan medical databases.

Database	Data source	Data type	Amount of data	Availability
Physionet	[121]	EEG, x-ray images, polysomnographic,	<i>Auditory evoked potential EEG-Biometric dataset</i> – 240 measurements from 20 subjects <i>The Brno University of Technology Smartphone PPG Database (BUT PPG)</i> – 12 polysomnographic recordings <i>CAP Sleep Database</i> - 108 polysomnographic recordings <i>CheXmask Database: a large-scale dataset of anatomical segmentation masks for chest x-ray images</i> – 676 803 chest radiographs <i>Electroencephalogram and eye-gaze datasets for robot-assisted surgery performance evaluation</i> – EEG from 25 subjects <i>Siena Scalp EEG Database</i> – EEG from 14 subjects	Publics
Physionet	[121]	EEG, x-ray images, polysomnographic,	<i>Computed Tomography Images for Intracranial Hemorrhage Detection and Segmentation</i> – 82 CT After Traumatic Brain Injury (TBI) <i>A multimodal dental dataset facilitating machine learning research and clinic service</i> -574 CBCT images from 389 patients <i>KURIAS-ECG: a 12-lead electrocardiogram database with standardized diagnosis ontology</i> - EEG 147 subjects <i>VinDr-PCXR: An open, large-scale pediatric chest X-ray dataset for interpretation of common thoracic diseases</i> – adult chest radiography (CXR) 9125 subjects <i>VinDr-SpineXR: A large annotated medical image dataset for spinal lesions detection and classification from radiographs</i> - 10466 spine X-ray images from 5000 studies	Restricted access
National Sleep Research Resource	[122]	Polysomnography	<i>Apnea Positive Pressure Long-term Efficacy Study</i> – 1516 subject <i>Efficacy Assessment of NOP Agonists in Non-Human Primates</i> – 5 subjects <i>Maternal Sleep in Pregnancy and the Fetus</i> – 106 subjects <i>Apnea, Bariatric surgery, and CPAP study</i> – 49 subjects <i>Best Apnea Interventions in Research</i> – 169 subjects <i>Childhood Adenotonsillectomy Trial</i> – 1243 subjects <i>Cleveland Children's Sleep and Health Study</i> – 517 subjects <i>Cleveland Family Study</i> – 735 subjects <i>Cox &amp; Fell (2020) Sleep Medicine Reviews</i> – 3 subjects <i>Heart Biomarker Evaluation in Apnea Treatment</i> – 318 subjects <i>Hispanic Community Health Study / Study of Latinos</i> – 16415 subjects <i>Home Positive Airway Pressure</i> – 373 subjects <i>Honolulu-Asia Aging Study of Sleep Apnea</i> – 718 subjects <i>Learn</i> – 3 subjects <i>Mignot Nature Communications</i> – 3000 subjects <i>MrOS Sleep Study</i> – 2237 subjects <i>NCH Sleep DataBank</i> – 3673 subjects <i>Nulliparous Pregnancy Outcomes Study Monitoring Mothers-to-be</i> – 3012 subjects <i>Sleep Heart Health Study</i> – 5804 subjects <i>Stanford Technology Analytics and Genomics in Sleep</i> – 1881 subjects <i>Study of Osteoporotic Fractures</i> – 461 subjects <i>Wisconsin Sleep Cohort</i> – 1123 subjects	Publics on request (no commercial use)
Open Access Series of Imaging Studies - Oasis Brain	[123]	MRI Alzheimer's disease	OASIS-1 – 416 subjects OASIS-2 – 150 subjects OASIS-3 – 1379 subjects OASIS-4 – 663 subjects	Publics on request (no commercial use)
openneuro	[124]	MRI, PET, MEG, EEG, and iEEG data (various types of disorders, depending on the database)	595 MRI public datasets, 23 304 subjects 8 PET public datasets – 19 subjects 161 EEG public dataset – 6790 subjects 23 iEEG public dataset – 550 subjects 32 MEG public dataset – 590 subjects	Publics
brain tumor dataset	[125]	MRI, brain tumor	MRI - 233 subjects	Publics
Cancer Imaging Archive (TCIA)	[126]	MR, CT, Positron Emission Tomography, Computed Radiography, Digital Radiography, Nuclear Medicine, Other (a category	HNSCC-mIF-mIHC-comparison – 8 subjects CT-Phantom4Radiomics – 1 subject Breast-MRI-NACT-Pilot – 64 subjects Adrenal-ACC-Ki67-Seg – 53 subjects CT Lymph Nodes – 176 subjects UCSF-PDGM – 495 subjects	Publics (Free access, registration required)

		used in DICOM for images that do not fit into the standard modality categories), Structured Reporting Pathology Various	UPENN-GBM – 630 subjects Hungarian-Colorectal-Screening – 200 subjects Duke-Breast-Cancer-MRI – 922 subjects Pancreatic-CT-CBCT-SEG – 40 subjects HCC-TACE-Seg – 105 subjects Vestibular-Schwannoma-SEG – 242 subjects ACRIN 6698/I-SPY2 Breast DWI – 385 subjects I-SPY2 Trial – 719 subjects HER2 tumor ROIs – 273 subjects DLBCL-Morphology – 209 subjects CDD-CESM – 326 subjects COVID-19-NY-SBU – 1,384 subjects Prostate-Diagnosis – 92 subjects NSCLC-Radiogenomics – 211 subjects CT Images in COVID-19 – 661 subjects QIBA-CT-Liver-Phantom – 3 subjects Lung-PET-CT-Dx – 363 subjects QIN-PROSTATE-Repeatability – 15 subjects NSCLC-Radiomics – 422 subjects Prostate-MRI-US-Biopsy – 1151 subjects CRC_FFPPE-CODEX_CellNeighs – 35 subjects TCGA-BRCA – 139 subjects TCGA-LIHC – 97 subjects TCGA-LUAD – 69 subjects TCGA-OV – 143 subjects TCGA-KIRC – 267 subjects Lung-Fused-CT-Pathology – 6 subjects AML-Cytomorphology_LMU – 200 subjects Pelvic-Reference-Data – 58 subjects CC-Radiomics-Phantom-3 – 95 subjects MiMM_SBILab – 5 subjects LCTSC – 60 subjects QIN Breast DCE-MRI – 10 subjects Osteosarcoma Tumor Assessment – 4 subjects CBIS-DDSM – 1566 subjects QIN LUNG CT – 47 subjects CC-Radiomics-Phantom – 17 subjects PROSTATEx – 346 subjects Prostate Fused-MRI-Pathology – 28 subjects SPIE-AAPM Lung CT Challenge – 70 subjects ISPY1 (ACRIN 6657) – 222 subjects Pancreas-CT – 82 subjects 4D-Lung – 20 subjects Soft-tissue-Sarcoma – 51 subjects LungCT-Diagnosis – 61 subjects Lung Phantom – 1 subject Prostate-3T – 64 subjects LIDC-IDRI – 1010 subjects RIDER Phantom PET-CT – 20 subjects RIDER Lung CT – 32 subjects BREAST-DIAGNOSIS – 88 subjects CT COLONOGRAPHY (ACRIN 6664) – 825 subjects	
LUNA16	[127]	CT, Lung Nodules	LUNA16- 888 CT scans	Publics (Free access to all users)
MICCAI 2012 Prostate Challenge	[128]	MRI, Prostate Imaging	Prostate Segmentation in Transversal T2-weighted MR images - Amount of Data: 50 training cases	Publics (Free access to all users)
IEEE Data-port	[129]	Ultrasound Images, Brain MRI, Ultra-widefield fluorescein angiography images, Chest X-rays, Mammograms, CT, Lung Image Database Consortium and Image, Thermal Images	CNN-Based Image Reconstruction Method for Ultrafast Ultrasound Imaging: 31,000 images OpenBHB: A Multi-Site Brain MRI Dataset for Age Prediction and Debiasing: >5,000 - Brain MRI. Benign Breast Tumor Dataset: 83 patients - Mammograms. X-ray Bone Shadow Suppression: 4,080 images STROKE: CT series of patients with M1 thrombus before thrombectomy: 88 patients Automatic lung segmentation results Nextmedproject - 718 of the 1012 LIDC-IDRI scans PRIME-FP20: Ultra-Widefield Fundus Photography Vessel Segmentation Dataset -15 images Plantar Thermogram Database for the Study of Diabetic Foot Complications - Amount of data: 122 subjects (DM group) and 45 subjects (control group)	A part Public and a part restricted (Subscription)
AIMI	[130]	Brain MRI studies, Chest X-rays, echocardiograms, CT	BrainMetShare- 156 subjects CheXlocalize: 700 subjects BrainMetShare: 156 subjects	Publics (Free access)

			COCA - Coronary Calcium and Chest CTs: Not specified CT Pulmonary Angiography: Not specified CheXlocalize: 700 subjects CheXpert: 65,240 subjects CheXphoto: 3,700 subjects CheXplanation: Not specified DDI - Diverse Dermatology Images: Not specified EchoNet-Dynamic: 10,030 subjects EchoNet-LVH: 12,000 subjects EchoNet-Pediatric: 7,643 subjects LERA - Lower Extremity Radiographs: 182 subjects MRNet: 1,370 subjects MURA: 14,863 studies Multimodal Pulmonary Embolism Dataset: 1,794 subjects SKM-TEA: Not specified Thyroid Ultrasound Cine-clip: 167 subjects CheXpert: 224,316 chest radiographs of 65,240 subjects	
fast MRI	[131]	MRI	fast MRI Knee: 1,500+ subjects  fast MRI Brain: 6,970 subjects  fast MRI Prostate: 312 subjects	Publics (Free access, registration required)
ADNI	[132]	MRI, PET	Scans Related to Alzheimer's Disease	Publics (Free access, registration required)
Pediatric Brain Imaging Data-set	[133]	MRI	Pediatric Brain Imaging Data-set Over 500 pediatric brain MRI scans	Publics (Free access to all users)
ChestX-ray8	[134]	Chest X-ray Images	NIH Clinical Center Chest X-ray Dataset - Over 100,000 images from more than 30,000 subjects	Publics (Free access to all users)
Breast Cancer Digital Repository	[135]	MLO and CC images	BCDR-FM (Film Mammography-based Repository) - Amount of Data: 1010 subjects BCDR-DM (Full Field Digital Mammography-based Repository)Amount of Data: 724 subjects	Publics (Free access, registration required)
Brain-CODE	[136]	Neuroimaging	High-Resolution Magnetic Resonance Imaging of Mouse Model Related to Autism - 839 subjects	Restricted (Application for access is required and Open Data Releases)
RadImage-Net	[137]	PET, CT, Ultrasound, MRI with DICOM tags	5 million images from over 1 million studies across 500,000 subjects	Publics subset available; Full dataset licensable; Academic access with restrictions
EyePACS	[138]	Retinal fundus images for diabetic retinopathy screening	Images for Training and validation set- 57,146 images Test set - 8,790 images	Available through the Kaggle competition
Medical Segmentation Decathlon	[139]	mp-MRI, MRI, CT	10 data sets Cases (Train/Test) Brain 484/266 Heart 20/10 Hippocampus 263/131 Liver 131/70 Lung 64/32 Pancreas 282/139 Prostate 32/16 Colon 126/64 Hepatic Vessels 303/140 Spleen 41/20	Open source license, available for research use
DDSM	[140]	Mammography images	2,500 studies with images, subjects info - 2620 cases in 43 volumes categorized by case type	Publics (Free access)
LIDC-IDRI	[141]	CT Images with Annotations	1018 cases with XML and DICOM files - Images (DICOM, 125GB), DICOM Metadata Digest (CSV, 314 kB), Radiologist Annotations/Segmentations (XML format, 8.62 MB), Nodule Counts by Patient (XLS), Patient Diagnoses (XLS)	Images and annotations are available for download with NBIA Data Retriever, usage under CC BY 3.0

synapse	[142]	CT scans, Zip files for raw data, registration data	CT scans- 50 scans with variable volume sizes and resolutions Labeled organ data -13 abdominal organs were manually labeled Zip files for raw data - Raw Data: 30 training + 20 testing; Registration Data: 870 training-training + 600 training-testing pairs	Under IRB supervision, Available for participants
Mini-MIAS	[143]	Mammographic images	322 digitized films on 2.3GB 8mm tape - Images derived from the UK National Breast Screening Programme and digitized with Joyce-Loebl scanning micro-densitometer to 50 microns, reduced to 200 microns and standardized to 1024x1024 pixels for the database	free for scientific research under a license agreement
Breast Cancer Histopathological Database (BreakHis)	[144]	microscopic images of breast tumor	9,109 microscopic images of breast tumor tissue collected from 82 subjects	free for scientific research under a license agreement
Messidor	[145]	eye fundus color numerical images	1200 eye fundus color numerical images of the posterior pole	free for scientific research under a license agreement

## 8. Discussion and conclusions

The most commonly used neural networks in the field of medicine are CNNs and ANNs, see **Table 1**. Moreover, the combination of Transformers and CNNs as well as GAN allows users to achieve increasingly more accurate results, these methods require refinement. It is also worth noting that the diagnostics processes require the interpretation of visual scenes, and here GNNs-based solutions like scene graphs [200] and knowledge graphs [201] may be beneficial. It is also important to remember that GNNs are designed to perform tasks that neural networks like CNN cannot perform. SIRENs seem also to be an interesting solution. What was surprising was the fact that many works on the use of Machine Learning do not contain a detailed description of the neural network architecture and the description of learning, even the description of the data sets is very general (i.e. treats AI as a black box), which are key issues responsible for the accuracy and reliability of the approach used. The effectiveness of learning algorithms is compared among others in terms of the number of learning cycles, number of objective function calculations, number of floating-point multiplications, computation time, and sensitivity to local minima. In addition to the selection of appropriate parameters and network structure, the selection of an appropriate (effective) network learning algorithm is of key importance. The most commonly applied learning algorithm in ANNs is backpropagation, however, it has a rather slow convergence rate and as a consequence, ANN has more redundancy [146]. On the other hand, the training of the SNNs due to quite complicated dynamics and the non-differentiable nature of the spike activity remains a challenge [147]. The three types of ANN and SNN learning rules can be distinguished: unsupervised learning, indirect, supervised learning, and direct supervised learning. Thus, a commonly used learning algorithm in SNNs is the arithmetic rule SpikePropo, which is similar in concept to the backpropagation (BP) algorithm, in which network parameters are iteratively updated in a direction to minimize the difference between the final outputs of the network and target labels [148, 149]. The main difference between SNNs and ANNs is output dynamics. However, arithmetic-based learning rules are not a good choice for building biologically efficient networks. Other learning methods have been proposed for this purpose, including bio-inspired algorithms like spike-timing-dependent plasticity [150], spike-driven synaptic plasticity [151], and the tempotron learning rule [65, 76, 77]. STDP is unsupervised learning, which characterizes synaptic changes solely in terms of the temporal contiguity of presynaptic spikes and postsynaptic potentials or spikes [152], while spike-driven synaptic plasticity is supervised learning and uses rate coding. However, still, ANN with BP learning achieves a better classification performance than SNNs trained with STDP. To obtain better performance the combination of layer-wise STDP-based unsupervised and supervised spike-based BP was proposed [153, 154]. Other commonly used learning algorithms are ReSuMe [57], and Chronotron [58]. The tempotron learning rule implements gradient-descent dynamics, which minimizes a cost function that measures the amount by which the maximum voltage generated by erroneous patterns deviates from the firing threshold. Tempotron learning is efficient in learning spiking patterns where information is embedded in precise timing spikes (temporal coding). Instead, [155] proposed a neuron normalization technique and an explicitly iterative neuron model, which resulted in a significant increase in the SNNs' learning rate. However, training the network still requires a lot of labeled samples (input data). Another learning algorithm is indirect. It firstly trains ANN (created with perceptron's) and thereupon transforms it into its SNN version with the same network structure (i.e., ANN-SNN conversion) [156]. The disadvantage of such learning is the fact, that reliably estimating frequencies requires a nontrivial passage of time, and this learning rule fails to capture the temporal dynamics of a spiking system. The most popular direct supervised learning is gradient descent, which uses the first-spike time to encode input [157]. It uses the first-spike time to encode input signals and minimizes the difference between the network output and desired signals, the whole process of which is similar to the traditional BP. Thus, the application of the temporal coding-based learning rule, which could potentially carry the same information efficiently using less number of spikes than the rate coding, can help to increase the speed of calculations. On the other hand, active learning methods, including bio-inspired active learning (BAL), bio-inspired active learning on Firing Rate (BAL-FR), and bio-inspired active learning on membrane potential (BAL-M) have been proposed to reduce the size of the input data [158]. During the learning procedure, the labeled data sets are used to train the empirical behaviors of patterns, while the generalization behavior of patterns is extracted from unlabeled data sets. It leverages the difference between empirical and generalization behavior patterns to select the samples unmatched by the known patterns. This approach is based on the behavioral pattern differences of neurons in SNNs for active sample selection, and can effectively reduce the sample size required for SNNs training.

The impact of a bio-inspired AI-based system in clinical practice has significant potential for clinicians and medical experts. As can be clearly observed, further directions of development of Artificial Intelligence are leaning towards elaboration of not treating it as a black box and the development of Biological Artificial Intelligence, i. e. using neuron models that accurately reproduce experimentally measured values, understanding how information is transmitted, encoded and processed in the brain and mapping it

in learning algorithms. The main issue is how replicated the architecture of the human brain and the mechanisms governing it. Biologically realistic large-scale brain models require a huge number of neurons as well as connections between them. Estimation of the behavior of a neuron network requires accurate models of the individual neurons along with accurate characterizations of the connections among them. In general, these models should contain all essential qualitative mechanisms and should provide results consistent with experimental physiological data. To fully characterize and predict the behavior of an identified network, one would need to know this architecture as well as any external currents or driving forces, and afferent input, applied to this network. Thus, the information transmission efficiency essentially depends on how neurons cooperate in the transfer process. The specific network architecture i.e. presence and distribution of long-range connections and the influence of inhibitor neurons, in particular the appropriate balance between excitatory and inhibitory neurons, make information transmission more effective [170]. Taking all these factors into account will put insight into the understanding of what factors contribute to the fact that the human brain is such a perfect computing machine. Then these mechanisms can be translated into the improvement of AI methods [171]. Moreover, it will put insight into the development of the next-generation AI, including Autonomous AI (AAI) as well as the development of brain simulators that balance computational complexity, energy efficiency, biological plausibility, and intellectual competence.

The second issue is connected with the so-called open data policy [211]. However, the publicly available datasets are not numerous, very often not labeled, described very generally, subject to bias, and additionally burdened with segmentation errors.

Another trend, which can be also observed is connected with the compliance of Artificial Intelligence with human rights, bioethics principles, and universal human values, which is especially important in medicine. For example, in Germany, a patient must give informed consent to the use of AI in the process of his diagnosis and treatment, which we believe is a good practice. Also, rules that should be fulfilled by the AI-based system like the Assessment List for Trustworthy Artificial Intelligence (ALTAI) [173-175], were formulated. In [163, 176] 10 ethical risk points (ERP) important to institutions, policymakers, teachers, students, and patients, including potential impacts on design, content, delivery, and AI-human-communication in the field of AI and Metaverse-based medical education were defined. Moreover, links are made between technical risks and ethical risks have been made. Now procedures need to be developed to enable their practical enforcement.

Thus, the integration of AI and Metaverse is a fact and suggests that AI may become the dominant approach for image scan segmentation and intelligent visual-content generation in the whole virtual world, not just medical applications [6, 159]. Recently, the Segment Anything Model (SAM) based on AI was introduced for natural images [89], in [160] SAM was proposed to be applied to medical images with a high level of accuracy. Better image segmentation contributes the higher-quality virtual objects. AI application in the context of the Metaverse is connected with the identification and categorization of meta-verse virtual items [161]. Moreover, AI may lead to more efficient cybersecurity solutions in the virtual world [162]. However, this is closely related to the accuracy of AI-based algorithms and, consequently, the accuracy of their training.

**Supplementary Materials:** Not applicable.

**Author Contributions:** “Conceptualization, A.P., and J.S.; methodology, A.P., J.S., and Z.R.; software, A.P., Z. R.; formal analysis, A.P., J.S., and Z.R.; investigation, A.P., J.S., and Z.R.; resources, A.P. and Z.R.; data curation, A.P., and Z.R.; writing—original draft preparation, A.P., and Z.R.; writing—review and editing, A.P., J.S., and Z.R.; visualization, A.P., and Z.R.; supervision, A.P.; project administration, A.P.; funding acquisition, J.S. All authors have read and agreed to the published version of the manuscript.”

**Funding:** “This research received no external funding”.

**Data Availability Statement:** Not applicable.

**Acknowledgments:** This study was partially supported by the National Centre for Research and Development (research grant Infostrateg I/0042/2021-00).

**Conflicts of Interest:** “The authors declare no conflict of interest.”

## References

1. Herculano-Houzel, S. The remarkable, yet not extraordinary, human brain as a scaled-up primate brain and its associated cost. *Proc. Natl. Acad. Sci. U S A* 2012, 109, pp. 10661-10668. <https://doi.org/10.1073/pnas.1201895109>.
2. Shao, F.; Shen, Z. How can artificial neural networks approximate the brain? *Front. Psychol.* 2023, Jane 9, pp 13:970214. <https://doi.org/10.3389/fpsyg.2022.970214>.
3. Moscato, V.; Napolano, G.; Postiglione, M. et al. Multi-task learning for few-shot biomedical relation extraction. *Artif. Intell. Rev.* 2023. [Online ahead of print]. Available online: <https://doi.org/10.1007/s10462-023-10484-6> (accessed 21 October 2023).
4. Wang, J.; Chen, S.; Liu, Y.; Lau, R. Intelligent Metaverse Scene Content Construction. *IEEE Access* 2023, 11, pp. 76222-76241.
5. López-Ojeda, W.; Hurley, R.A. Digital Innovation in Neuroanatomy: Three-Dimensional (3D) Image Processing and Printing for Medical Curricula and Health Care. *J. Neuropsychiatry Clin. Neurosci.* 2023, 35, pp. 206-209.
6. Kim, E.J.; Kim, J.Y. The Metaverse for Healthcare: Trends, Applications, and Future Directions of Digital Therapeutics for Urology. *Int. Neurorol. J.* 2023, 27, pp. S3-S12. <https://doi.org/10.5213/inj.2346108.054>.
7. Pregowska, A.; Osial, M.; Dolega-Dolegowski, D.; Kolecki, R.; Proniewska, K. Information and Communication Technologies Combined with Mixed Reality as Supporting Tools in Medical Education. *Electronics* 2023, 11, 3778. <https://doi.org/10.3390/electronics11223778>.
8. Fang, X.; Yan, P. Multi-organ segmentation over partially labeled datasets with multi-scale feature abstraction. *IEEE Trans. Med. Imaging* 2020, 39, pp. 3619-3629.
9. Yuan, F.; Zhang, Z.; Fang, Z. An Effective CNN and Transformer Complementary Network for Medical Image Segmentation. *Pattern Recognit.* 2023, 136, 109228. <https://doi.org/10.1016/j.patcog.2022.109228>.
10. Mazurowski, M.A.; Dong, H.; Gu, H.; Yang, J.; Konz, N.; Zhang, Y. Segment anything model form medical image analysis: An experimental study. *Med. Image Anal.* 2023, 89, 102918. <https://doi.org/10.1016/j.media.2023.102918>.

11. Sakshi, S.; Kukreja, V.; Image Segmentation Techniques: Statistical, Comprehensive, Semi-Automated Analysis and an Application Perspective Analysis of Mathematical Expressions. *Arch. Computat. Methods Eng.* 2023, 30, pp. 457–495.
12. Moztarzadeh, O.; Jamshidi, M.; Sargolzaei, S.; Keikhaee, F.; Jamshidi, A.; Shadroo, S.; Hauer, L. Metaverse and Medical Diagnosis: A Blockchain-Based Digital Twinning Approach Based on MobileNetV2 Algorithm for Cervical Vertebral Maturation. *Diagnostics.* 2023, 13, 1485.
13. Huynh-The, T.; Pham, Q.-V.; Pham, M.-T.; Banh, T.-N.; Nguyen, G.-P.; Kim, D.-S. Efficient Real-Time Object Tracking in the Metaverse Using Edge Computing with Temporal and Spatial Consistency. *Comput. Mater. Contin.* 2023, 71, pp. 341–356.
14. Huang, H.; Zhang, C.; Zhao, L.; Ding, S.; Wang, H.; Wu, H. Self-Supervised Medical Image Denoising Based on WISTA-Net for Human Healthcare in Metaverse. *IEEE J. Biomed. Health Inform.* pp. 1–9 2023.
15. The PRISMA 2020 Statement: an updated guideline for reporting systematic reviews (published in several journals) <http://www.prisma-statement.org/PRISMAStatement/PRISMAStatement>, 2021
16. Rethlefsen, M.L.; Kirtley, S.; Waffenschmidt, S.; Ayala, A.P.; Moher, D.; Page, M.J.; Koffel, J.B. PRISMA-S: An Extension to the PRISMA Statement for Reporting Literature Searches in Systematic Reviews. *Syst. Rev.* 2021, 10, 39.
17. Adrian, E.D.; Zotterman, Y. The Impulses Produced by Sensory Nerve Endings. *J. Physiol.* 1926, 61, pp. 465–483. <https://doi.org/10.1113/jphysiol.1926.sp002281>.
18. Gerstner, W.; Kistler, W.M.; Naud, R.; Paninski, L. *Neuronal Dynamics: From Single Neurons to Networks and Models of Cognition*. Cambridge University Press, Cambridge, UK, 2014.
19. Rieke, F.; Warland, D.; de Ruyter van Steveninck, R.; Bialek, W. *Spikes: Exploring the Neural Code*. The MIT Press: Cambridge, MA, USA, 1997.
20. van Hemmen, J.L.; Sejnowski, T.J. *23 Problems in Systems Neuroscience*. Oxford University Press: Oxford, UK, 2006.
21. Teich, M.C.; Khanna, S.M. Pulse-Number distribution for the neural spike train in the cat's auditory nerve. *J. Acoust. Soc. Am.* 1985, 77, pp. 1110–1128.
22. Werner, G.; Mountcastle, V.B. Neural activity in mechanoreceptive cutaneous afferents: stimulus-response relations, Weber Functions, and Information Transmission. *J. Neurophysiol.* 1965, 28, pp. 359–397
23. Tolhurst, D.J.; Movshon, J.A.; Thompson, I.D. The dependence of Response amplitude and variance of cat visual cortical neurons on stimulus contrast. *Exp. Brain Res.* 1981, 41, pp. 414–419.
24. Radons, G.; Becker, J.D.; Dülfer, B.; Krüger, J. Analysis, classification, and coding of multielectrode spike trains with hidden Markov models. *Biol. Cybern.* 1994, 71, pp. 359–373.
25. de Ruyter van Steveninck, R.R.; Lewen, G.D.; Strong, S.P.; Koberle, R.; Bialek, W. Reproducibility and variability in neural spike trains. *Science* 1997, 275, pp. 1805–1808.
26. Kass, R.E.; Ventura, V. A spike-train probability model. *Neural Comput.* 2001, 13, pp. 1713–1720.
27. Wójcik, D. The kinematics of the spike trains. *Acta Phys. Pol. B.* 2018, 49, pp. 2127–2138.
28. Rosenblatt, F. Principles of neurodynamics. Perceptrons and the theory of Bbain mechanisms. *Tech. Rep., Cornell Aeronautical Lab Inc*, Buffalo, NY, USA, 1961
29. Bu, T.; Fang, W.; Ding, J.; Dai, P.L.; Yu, Z.; Huang, T. Optimal ANN-SNN Conversion for High-Accuracy and Ultra-Low-Latency Spiking Neural Networks. *arXiv preprint arXiv:2303.04347*, 2023. Available online: <https://doi.org/10.48550/arXiv.2303.04347> (accessed on January 4).
30. Abbott, L.F.; Dayan, P. *Theoretical Neuroscience Computational and Mathematical Modeling of Neural Systems*, The MIT Press, 2000.
31. Yuan, Y.; Gao, R.; Wu, Q.; Fang, S.; Bu, X.; Cui, Y.; Han, C.; Hu, L.; Li, X.; Wang, X.; Geng, L.; Liu, W. Artificial Leaky Integrate-and-Fire Sensory Neuron for In-Sensor Computing Neuromorphic Perception at the Edge. *ACS Sensors* 2023, 8 (7), 2646–2655.
32. Ghosh-Dastidar, S.; Adeli, H. *Third Generation Neural Networks: Spiking Neural Networks*. In *Advances in Computational Intelligence*; Yu, W.; Sanchez, E.N., Eds.; Springer: Berlin, Heidelberg, 2009; Volume 116.
33. Lindeberg, T. A time-causal and time-recursive scale-covariant scale-space representation of temporal signals and past time. *Biol. Cybern.* 2023, 117, pp. 21–59. PMID: 36689001 PMCID: PMC10160219.
34. Rueckauer, B.; Lungu, I.A.; Hu, Y.; Pfeiffer, M.; Liu, S.C. Conversion of Continuous-Valued Deep Networks To Efficient Event-Driven Neuromorphic Hardware. *Front. Neurosci.* 2017, 11.
35. Cheng, X.; Zhang, T.; Jia, S.; Xu, B. Meta neurons improve spiking neural networks for efficient spatio-temporal learning. *Neurocomputing* 2023, 531, pp. 217–225.
36. LeCun, Y.; Bottou, L.; Bengio, Y.; Haffner, P. Gradient-based learning applied to document recognition. *Proc. IEEE*, 1998, 86, pp. 2278–2324.
37. Mehrishi, A.; Majumder, N.; Bharadwaj, R.; Mihalcea, R.; Poria, S. A review of deep learning techniques for speech processing. *Inf. Fusion* 2023, 99, 101869. <https://doi.org/10.1016/j.inffus.2023.101869>.
38. Nielsen, M.A. *Neural Networks and Deep Learning*. Determination Press, 2015; eBook. Available online: [NeuralNetworksAndDeepLearning.com](http://neuralnetworksanddeeplearning.com) (accessed on January 8, 2024).
39. Yamashita, R.; Nishio, M.; Do, R.K.G.; et al. Convolutional neural networks: an overview and application in radiology. *Insights Imaging* 2018, 9, pp. 611–629. <https://doi.org/10.1007/s13244-018-0639-9>.
40. Sherstinsky, A. Fundamentals of Recurrent Neural Network (RNN) and Long Short-Term Memory (LSTM) network. *Physica D: Non-linear Phenomena*, 2020, 404, 132306. <https://doi.org/10.1016/j.physd.2019.132306>.
41. Ghosh-Dastidar, S.; Adeli, H. Spiking neural networks. *Int. J. Neural Syst.* 2009, 19, pp. 295–308.
42. Yamazaki, K.; Vo-Ho, V.K.; Bulsara, D.; Le, N. Spiking Neural Networks and Their Applications: A Review. *Brain Sci.* 2022, 12b, 863.
43. Dampfhofer, A.; et al. Backpropagation-Based Learning Techniques for Deep Spiking Neural Networks: A Survey. *IEEE Trans. Neural Netw. Learn. Syst.* 2023, 1–16.
44. Ponulak, F.; Kasinski, A. Introduction to spiking neural networks: Information processing, learning and applications. *Acta Neurobiol Exp (Wars)*. 2011, 71, 409–33.
45. Wu, Y.; et al. Spatio-Temporal Backpropagation for Training High-Performance Spiking Neural Networks. *Front Neurosci.* 2018, 12, 331.
46. Pei, J.; Deng, L.; Song, S.; Zhao, M.; Zhang, Y.; Wu, S.; Wang, G.; Zou, Z.; Wu, Z.; He, W.; et al. Towards artificial general intelligence with hybrid Tianjic chip architecture. *Nature* 2019, 572, 106–111.

47. Rathi, N.; Chakraborty, I.; Kosta, A.; Sengupta, A.; Ankit, A.; Panda, P.; Roy, K. Exploring Neuromorphic Computing Based on Spiking Neural Networks: Algorithms to Hardware. *ACM Comput. Surv.* 2023, 55, 243.
48. Rojas, R. The Backpropagation Algorithm. In *Neural Networks*; Springer: Berlin, Heidelberg, 1996; pp. 1-50.
49. Singh, A.; Kushwaha, S.; Alarfaj, M.; Singh, M. Comprehensive Overview of Backpropagation Algorithm for Digital Image Denoising. *Electronics* 2022, 11, 1590.
50. Kaur, J.; Khehra, B.S.; Singh, A. Back propagation artificial neural network for diagnosis of heart disease. *J. Reliable Intell. Environ.* 2023, 9, PP. 57–85.
51. Hameed, A.A.; Karlik, B.; Salman, M. S. Back-propagation algorithm with variable adaptive momentum. *Knowledge-Based Systems* 2016, 114, 79–87.
52. Cao, Y.; Chen, Y.; Khosla, D. Spiking Deep Convolutional Neural Networks for Energy-Efficient Object Recognition. *Int. J. Comput. Vis.* 2015, 113, 54–66.
53. Alemanno, F.; Aquaro, M.; Kanter, I.; Barra, A.; Agliari, E. Supervised Hebbian Learning. *Europhys. Lett.* 2023, 141, 11001. <https://doi.org/10.1209/0295-5075/aca55f>.
54. Ponulak, F. ReSuMe—New Supervised Learning Method for Spiking Neural Networks. Technical Report, Technical Report, Poznań University of Technology, Poznań, Poland, 2005. <https://www.semanticscholar.org/paper/ReSuMe-New-Supervised-Learning-Method-for-Spiking-Ponulak/b04f2391b8c9539edff41065c39fc2d27cc3d95a>
55. Shrestha, A.; Ahmed, K.; Wang, Y.; Qiu, Q. Stable Spike-Timing Dependent Plasticity Rule for Multilayer Unsupervised and Supervised Learning. In Proceedings of the 2017 International Joint Conference on Neural Networks (IJCNN), Anchorage, AK, USA, 14–19 May 2017, pp. 1999–2006. <https://doi.org/10.1109/IJCNN.2017.7966096>.
56. Amato, G.; Carrara, F.; Falchi, F.; Gennaro, C.; Lagani, G. Hebbian Learning Meets Deep Convolutional Neural Networks. In *Image Analysis and Processing – ICIAP 2019*; Ricci, E., Rota Bulò, S., Snoek, C., Lanz, O., Messelodi, S., Sebe, N., Eds.; Lecture Notes in Computer Science, vol 11751 pp. 1-14, Springer: Cham, 2019. [https://doi.org/10.1007/978-3-030-30642-7\\_29](https://doi.org/10.1007/978-3-030-30642-7_29).
57. Ponulak, F.; Kasinski, A. Supervised learning in spiking neural networks with ReSuMe: sequence learning, classification, and spike shifting. *Neural Comput.* 2010, 22, 467–510. <https://doi.org/10.1162/neco.2009.11-08-901>.
58. Florian, R.V. The Chronotron: A Neuron That Learns to Fire Temporally Precise Spike Patterns. *PLoS One* 2012, 7, e40233. <https://doi.org/10.1371/journal.pone.0040233>.
59. Victor, J.D.; Purpura, K.P. Metric-space analysis of spike trains: theory, algorithms, and applications. *Network* 1997, 8, 127–164. [https://doi.org/10.1088/0954-898X\\_8\\_2\\_003](https://doi.org/10.1088/0954-898X_8_2_003).
60. Huang, C.; Wang, J.; Wang, S.-H.; Zhang, Y.-D. Applicable artificial intelligence for brain disease: A survey. *Neurocomputing* 2022, 504, pp. 223–239. <https://doi.org/10.1016/j.neucom.2022.07.005>.
61. Markram, H.; Gerstner, W.; Sjöström, P.J. A history of spike-timing-dependent plasticity. *Front. Synaptic Neurosci.* 2011, 3, 4, <https://doi.org/10.3389/fnsyn.2011.00004>.
62. Merolla, P.A.; et al. A million spiking-neuron integrated circuit with a scalable communication network and interface. *Science* 2014, 345, 668–673. <https://doi.org/10.1126/science.1254642>.
63. Chakraborty, B.; Mukhopadhyay, S. Characterization of Generalizability of Spike Timing Dependent Plasticity Trained Spiking Neural Networks. *Front. Neurosci.* 2021, 15, 695357. <https://doi.org/10.3389/fnins.2021.695357>.
64. Lagani, G.; Falchi, F.; Gennaro, C.; Amato, G. Spiking Neural Networks and Bio-Inspired Supervised Deep Learning: A Survey. *arXiv preprint arXiv:2307.16235*, 2023. Available online: <https://doi.org/10.48550/arXiv.2307.16235> (accessed on January 8, 2024).
65. Gütig, R.; Sompolinsky, H. The tempotron: a neuron that learns spike timing-based decisions. *Nat. Neurosci.* 2006, 9, pp. 420–428. <https://doi.org/10.1038/nn1643>.
66. Cellina, M.; Cè, M.; Ali, M.; Irmici, G.; Ibba, S.; Caloro, E.; Fazzini, D.; Oliva, G.; Papa, S. Digital Twins: The New Frontier for Personalized Medicine? *Appl. Sci.* 2023, 13, 7940. <https://doi.org/10.3390/app13137940>.
67. Sun, T.; He, X.; Li, Z. Digital twin in healthcare: Recent updates and challenges. *Digital Health* 2023, 9. <https://doi.org/10.1177/20552076221149651>.
68. Uhl, J.C.; Schrom-Feiertag, H.; Regal, G.; Gallhuber, K.; Tscheligi, M. Tangible Immersive Trauma Simulation: Is Mixed Reality the Next Level of Medical Skills Training? In: Proceedings of the 2023 CHI Conference on Human Factors in Computing Systems (CHI '23), New York, NY, USA, 2023; Association for Computing Machinery: New York, NY, USA, 2023; Article 513. <https://doi.org/10.1145/3544548.3581292>.
69. Kshatri, S.S.; Singh, D. Convolutional Neural Network in Medical Image Analysis: A Review. *Arch Computat Methods Eng.* 2023, 30, 2793–2810. <https://doi.org/10.1007/s11831-023-09898-w>.
70. Li, X.; Guo, Y.; Jiang, F.; Xu, L.; Shen, F.; Jin, Z.; Wang, Y. Multi-Task Refined Boundary-Supervision U-Net (MRBSU-Net) for Gastrointestinal Stromal Tumor Segmentation in Endoscopic Ultrasound (EUS) Images. *IEEE Access* 2020, 8, 5805–5816. <https://doi.org/10.1109/ACCESS.2019.2963472>.
71. Oktay, O.; Schlemper, J.; Le Folgoc, L.; Lee, M.; Heinrich, M.; Misawa, K.; Mori, K.; McDonagh, S.; Hammerla, N.Y.; Kainz, B. et al. Attention U-Net: Learning Where to Look for the Pancreas. 2018. *arXiv preprint arXiv:1804.03999*, Available <https://doi.org/10.48550/arXiv.1804.03999> (accessed on January 8, 2024).
72. Ronneberger, O.; Fischer, P.; Brox, T. U-Net: Convolutional Networks for Biomedical Image Segmentation. In *Medical Image Computing and Computer-Assisted Intervention – MICCAI 2015*; Navab, N., Hornegger, J., Wells, W.M., Frangi, A.F., eds.; Springer International Publishing: Cham, Switzerland, 2015, 234–241.
73. Zhou, Z.; Rahman Siddiquee, M.M.; Tajbakhsh, N.; Liang, J. UNet++: A Nested U-Net Architecture for Medical Image Segmentation. In *Deep Learning in Medical Image Analysis and Multimodal Learning for Clinical Decision Support*; Crimi, A., Bakas, S., Kuijf, H., Menze, B., Reyes, M., eds.; Springer International Publishing: Cham, Switzerland, 2018, 3–11.
74. Alom, M.Z.; Yakopcic, C.; Hasan, M.; Taha, T.M.; Asari, V.K. Recurrent residual U-Net for medical image segmentation. *J Med Imaging (Bellingham)* 2019, 6(1), 014006. <https://doi.org/10.1117/1.JMI.6.1.014006>.
75. Ren, Y.; Zou, D.; Xu, W.; Zhao, X.; Lu, W.; He, X. Bimodal segmentation and classification of endoscopic ultrasonography images for solid pancreatic tumor. *Biomed. Signal Process. Control.* 2023, 83, 104591. <https://doi.org/10.1016/j.bspc.2023.104591>.
76. Urbanczik, R.; Senn, W. Reinforcement learning in populations of spiking neurons. *Nat. Neurosci.* 2009, 12, 250–252. <https://doi.org/10.1038/nn.2264>.

77. Yu, Q.; Tang, H.; Tan, K. C.; Yu, H. A brain-inspired spiking neural network model with temporal encoding and learning. *Neurocomputing* 2014, 138, 3–13. <https://doi.org/10.1016/j.neucom.2013.06.052>.

78. Kumarasinghe, K.; Kasabov, N.; Taylor, D. Brain-inspired spiking neural networks for decoding and understanding muscle activity and kinematics from electroencephalography signals during hand movements. *Sci. Rep.* 2021, 11, 1–15. <https://doi.org/10.1038/s41598-021-81805-4>.

79. Niu, L.Y.; Wei, Y.; Liu, W.B.; et al. Research Progress of spiking neural network in image classification: A Review. *Appl. Intell.* 2023, 53, 19466–19490. <https://doi.org/10.1007/s10489-023-04553-0>.

80. Yuan, F.; Zhang, Z.; Fang, Z. An Effective CNN and Transformer Complementary Network for Medical Image Segmentation. *Pattern Recognition* 2023, 136, 109228. <https://doi.org/10.1016/j.patcog.2022.109228>.

81. Pregowska, A.; Osial, M.; Dolega-Dolegowski, D.; Kolecki, R.; Proniewska, K. Information and Communication Technologies Combined with Mixed Reality as Supporting Tools in Medical Education. *Electronics* 2022, 11(22), 3778. <https://doi.org/10.3390/electronics11223778>.

82. Proniewska, K.; Dolega-Dolegowski, D.; Kolecki, R.; Osial, M.; Pregowska, A. Applications of Augmented Reality - Current State of the Art, In The 3D Operating Room with Unlimited Perspective Change and Remote Support. InTech: Rijeka, Croatia, 2023, 1–23.

83. Suh, I.; McKinney, T.; Siu, K.-C. Current Perspective of Metaverse Application in Medical Education, Research and Patient Care. *Virtual Worlds* 2023, 2, 115–128. <https://doi.org/10.3390/virtualworlds2020007>.

84. Liu, X.; Song, L.; Liu, S.; Zhang, Y. A Review of Deep-Learning-Based Medical Image Segmentation Methods. *Sustainability* 2021, 13, 1224. <https://doi.org/10.3390/su13031224>.

85. Li, Y.; Zhang, Y.; Liu, J.-Y.; Wang, K.; Zhang, K.; Zhang, G.-S.; Liao, X.-F.; Yang, G. Global Transformer and Dual Local Attention Network via Deep-Shallow Hierarchical Feature Fusion for Retinal Vessel Segmentation. *IEEE Trans. Cybern.* 2022. <https://doi.org/10.1109/TCYB.2022.3194099>.

86. Chen, J.; Lu, Y.; Yu, Q.; Luo, X.; Adeli, E.; Wang, Y.; Lu, L.; Yuille, A.L.; Zhou, Y. TransUNet: Transformers Make Strong Encoders for Medical Image Segmentation. Available online arXiv preprint arXiv:2102.04306, 2021. Available online: <https://doi.org/10.48550/arXiv.2102.04306> (accessed on January 8, 2024).

87. Xiao, H.; Li, L.; Liu, Q.; Zhu, X.; Zhang, Q. Transformers in Medical Image Segmentation: A Review. *Biomed. Signal Process. Control.* 2023, 84(12), 104791. <https://doi.org/10.1016/j.bspc.2023.104791>.

88. Yu, H.; Yang, L.T.; Zhang, Q.; Armstrong, D.; Deen, M.J. Convolutional Neural Networks for Medical Image Analysis: State-of-the-Art, Comparisons, Improvement, and Perspectives. *Neurocomputing* 2021, 444, 92–110. <https://doi.org/10.1016/j.neucom.2020.04.157>.

89. Meta. <https://segment-anything.com/> (accessed on 13 November 2023).

90. Kirillov, A.; Mintun, E.; Ravi, N.; Mao, H.; Rolland, C.; Gustafson, L.; Xiao, T.; Whitehead, S.; Berg, A.C.; Lo, W.Y., et al. Segment Anything. arXiv preprint arXiv:2304.02643, 2023. Available online: <https://segment-anything> (accessed on January 8, 2024).

91. He, S.; Bao, R.; Li, J.; Stout, J.; Bjornerud, A.; Grant, P.E.; Ou, Y. Computer-Vision Benchmark Segment-Anything Model (SAM) in Medical Images: Accuracy in 12 Datasets. arXiv preprint arXiv:2304.09324, 2023; Available online: <https://arxiv.org/abs/2304.09324> (accessed on January 8, 2024).

92. Zhang, Y.; Jiao, R. Towards Segment Anything Model (SAM) for Medical Image Segmentation: A Survey. arXiv preprint arXiv:2305.03678, 2023; Available online: <https://arxiv.org/abs/2305.03678> (accessed on 13 November 2023).

93. Wu, J.; Zhang, Y.; Fu, R.; Fang, H.; Liu, Y.; Wang, Z.; Xu, Y.; Jin, Y. Medical SAM Adapter: Adapting Segment Anything Model for Medical Image Segmentation. arXiv preprint: arXiv:2304.12620, 2023; <https://arxiv.org/abs/2304.12620>, 2023 (accessed on January 8, 2024).

94. Yi, Z.; Lian, J.; Liu, Q.; Zhu, H.; Liang, D.; Liu, J. Learning Rules in Spiking Neural Networks: A Survey. *Neurocomputing* 2023, 531, 163–179. <https://doi.org/10.1016/j.neucom.2023.02.026>.

95. Avcı, H.; Karakaya, J. A Novel Medical Image Enhancement Algorithm for Breast Cancer Detection on Mammography Images Using Machine Learning. *Diagnostics* 2023, 13, 348. <https://doi.org/10.3390/diagnostics13030348>.

96. Ghahramani, M.; Shiri, N. Brain tumour detection in magnetic resonance Imaging using Levenberg–Marquardt backpropagation neural network. *IET Image Process.* 2023, 17, 88–103. <https://doi.org/10.1049/ipr2.12619>.

97. Zhang, J.; Gajjala, S.; Agrawal, P.; Tison, G. H.; Hallock, L. H.; Beussink-Nelson, L.; Lassen, M. H.; Fan, E.; Aras, M. A.; Jordan, C.; Fleischmann, K. E.; Melisko, M.; Qasim, A.; Shah, S. J.; Bajcsy, R.; Deo, R. C. Fully automated echocardiogram interpretation in clinical practice. *Circulation* 2018, 138, 1623–1635.

98. Sajjad, M.; Khan, S.; Khan M.; Wu, W.; Ullah, A.; Baik, S. W. Multi-grade brain tumor classification using deep CNN with extensive data augmentation. *Journal of Computational Science* 2021, 30, 174–182. <https://doi.org/10.1016/j.jocs.2018.12.003>.

99. Jun, T.J.; Kang, S.J.; Lee, J.G.; Kweon, J.; Na, W.; Kang, D.; Kim, D.; Kim, D.; Kim, Y.H. Automated detection of vulnerable plaque in intravascular ultrasound images. *Medical & biological engineering & computing* 2019, 57(4), 863–876. <https://doi.org/10.1007/s11517-018-1925-x>.

100. Ostvik, A.; Smistad, E.; Aase, S. A.; Haugen, B. O.; Lovstakken, L. Real-time standard view classification in transthoracic echocardiography using convolutional neural networks. *Ultrasound in medicine & biology* 2019, 45, 374–384. <https://doi.org/10.1016/j.ultrasmedbio.2018.07.024>.

101. Lossau, T.; Nickisch, H.; Wisse, T.; Bippus, R.; Schmitt, H.; Morlock, M.; Grass, M. Motion artifact recognition and quantification in coronary CT angiography using convolutional neural networks. *Medical image analysis* 2019, 52, 68–79. <https://doi.org/10.1016/j.media.2018.11.003>.

102. Emad, O.; Yassine, I. A.; Fahmy, A. S. Automatic localization of the left ventricle in cardiac MRI images using deep learning. In Conf Proc IEEE Eng. Med. Biol. Soc. 2015, 683–686. <https://doi.org/10.1109/EMBC.2015.7318454>.

103. Moradi, M.; Guo, Y.; Gur, Y.; Negahdar, M.; Syeda-Mahmood, T. A Cross-Modality Neural Network Transform for Semi-automatic Medical Image Annotation. In: Ourselin, S.; Joskowicz, L.; Sabuncu, M.; Unal, G.; Wells, W. (eds) *Medical Image Computing and Computer-Assisted Intervention – MICCAI 2016*. MICCAI 2016. Lecture Notes in Computer Science, vol 9901. Springer, Cham. [https://doi.org/10.1007/978-3-319-46723-8\\_35](https://doi.org/10.1007/978-3-319-46723-8_35).

104. Liskowski, P.; Krawiec, K. Segmenting retinal blood vessels with deep neural networks. *IEEE Trans Med Imaging* 2016, 35, 2369–2380. <https://doi.org/10.1109/TMI.2016.2546227>

105. Yuan, J.; Hassan, S.S.; Wu, J.; et al. Extended reality for biomedicine. *Nat Rev Methods Primers.* 2023, 3, 14. <https://doi.org/10.1038/s43586-023-00198-y>.

106. Kakhandaki, N.; Kulkarni, S.B. Classification of Brain MR Images Based on Bleed and Calcification Using ROI Cropped U-Net Segmentation and Ensemble RNN Classifier. *Int. J. Inf. Technol.* 2023, 15, 3405–3420. <https://doi.org/10.1007/s41870-023-01389-2>.

107. Manimurugan, S. Hybrid High Performance Intelligent Computing Approach of CACNN and RNN for Skin Cancer Image Grading. *Soft Comput.* 2023, 27, 579–589. <https://doi.org/10.1007/s00500-022-06989-x>.

108. Yue, Y.; Baltes, M.; Abuhamar, N.; Sun, T.; Karanth, A.; Smith, C.D.; Bihl, T.; Liu, J. Spiking Neural Networks Fine-Tuning for Brain Image Segmentation. *Front. Neurosci.* 2023, 17, 1267639. <https://doi.org/10.3389/fnins.2023.1267639>.

109. Liang, J.; Li, R.; Wang, C.; Zhang, R.; Yue, K.; Li, W.; Li, Y. A Spiking Neural Network Based on Retinal Ganglion Cells for Automatic Burn Image Segmentation. *Entropy* 2022, 24, 1526. <https://doi.org/10.3390/e24111526>

110. Gilani, S.Q.; Syed, T.; Umair, M. et al. Skin Cancer Classification Using Deep Spiking Neural Network. *J. Digit. Imaging.* 2023, 36, 1137–1147. <https://doi.org/10.1007/s10278-023-00776-2>.

111. Sahoo, A.K.; Parida, P.; Muralibabu, K.; Dash, S. Efficient Simultaneous Segmentation and Classification of Brain Tumors from MRI Scans Using Deep Learning. *Biocybernetics and Biomedical Engineering* 2023, 43(3), 616–633. <https://doi.org/10.1016/j.bbe.2023.08.003>.

112. Fu, Q.; Dong, H. Breast Cancer Recognition Using Saliency-Based Spiking Neural Network. *Wireless Communications and Mobile Computing* 2022, 2022, 8369368. <https://doi.org/10.1155/2022/8369368>.

113. Tan, P.; Chen, X.; Zhang, H.; Wei, Q.; Luo, K. Artificial intelligence aids in development of nanomedicines for cancer management. *Semin. Cancer Biol.* 2023, 89, 61–75. <https://doi.org/10.1016/j.semcaner.2023.01.005>.

114. Malhotra, S.; Halabi, O.; Dakua, S.P.; Padhan, J.; Paul, S.; Palliyali, W. Augmented Reality in Surgical Navigation: A Review of Evaluation and Validation Metrics. *Appl. Sci.* 2023, 13, 1629. <https://doi.org/10.3390/app13031629>.

115. Wisotzky, E.L.; Rosenthal, J-C.; Meij, S.; et al. Telepresence for surgical assistance and training using eXtended reality during and after pandemic periods. *J. Telemed. Telecare.* 2023, <https://doi.org/10.1177/1357633X231166226>.

116. Martin-Gomez, A.; et al. STTAR: Surgical Tool Tracking Using Off-the-Shelf Augmented Reality Head-Mounted Displays. *IEEE Trans. Vis. Comput. Graph.* 2022. <https://doi.org/10.1109/TVCG.2023.3238309>.

117. Minopoulos, G.M.; Memos, V.A.; Stergiou, K.D.; Stergiou, C.L.; Psannis, K.E. A Medical Image Visualization Technique Assisted with AI-Based Haptic Feedback for Robotic Surgery and Healthcare. *Appl. Sci.* 2023, 13, 3592. <https://doi.org/10.3390/app13063592>.

118. Li, J.; Cairns, B.J.; Li, J.; et al. Generating synthetic mixed-type longitudinal electronic health records for artificial intelligent applications. *Digit. Med.* 2023, 6, 98. <https://doi.org/10.1038/s41746-023-00834-7>.

119. Pammi, M.; Aghaeepour, N.; Neu, J. Multiomics, artificial intelligence, and precision medicine in perinatology. *Pediatr. Res.* 2023, 93, pp. 308–315. <https://doi.org/10.1038/s41390-022-02181-x>.

120. Vardi, G. On the Implicit Bias in Deep-Learning Algorithms. *Commun. ACM.* 2023, 66(6), pp. 86–93. <https://doi.org/10.1145/3571070>.

121. PhysioNet. Available online: <https://physionet.org/> (accessed on January 8, 2024).

122. National Sleep Research Resource. Available online: <https://sleepdata.org/> (accessed on January 8, 2024).

123. Open Access Series of Imaging Studies - OASIS Brain. Available online: <https://www.oasis-brains.org/> (accessed on January 8, 2024).

124. OpenNeuro. Available online: <https://openneuro.org/> (accessed on January 8, 2024).

125. Brain Tumor Dataset. Available online: [https://figshare.com/articles/dataset/brain\\_tumor\\_dataset/1512427?file=7953679](https://figshare.com/articles/dataset/brain_tumor_dataset/1512427?file=7953679) (accessed on January 8, 2024).

126. The Cancer Imaging Archive. Available online: <https://www.cancerimagingarchive.net/> (accessed on January 8, 2024).

127. LUNA16. Available online: <https://luna16.grand-challenge.org/> (accessed on January 8, 2024).

128. MICCAI 2012 Prostate Challenge. Available online: <https://promise12.grand-challenge.org/> (accessed on January 8, 2024).

129. IEEE Dataport. Available online: <https://ieee-dataport.org/> (accessed on January 8, 2024).

130. AIMI. Available online: <https://aimi.stanford.edu/shared-datasets> (accessed on January 8, 2024).

131. fastMRI. Available online: <https://fastmri.med.nyu.edu/> (accessed on January 8, 2024).

132. Alzheimer's Disease Neuroimaging Initiative. Available online: <http://adni.loni.usc.edu/> (accessed on January 8, 2024).

133. Pediatric Brain Imaging Dataset. Available online: [http://fcon\\_1000.projects.nitrc.org/indi/retro/pediatric.html](http://fcon_1000.projects.nitrc.org/indi/retro/pediatric.html) (accessed on January 8, 2024).

134. ChestX-ray8. Available online: <https://nihcc.app.box.com/v/ChestXray-NIHCC> (accessed on January 8, 2024).

135. Breast Cancer Digital Repository. Available online: <https://bcdr.eu/> (accessed on January 8, 2024).

136. Brain-CODE. Available online: <https://www.braincode.ca/> (accessed on January 8, 2024).

137. RadImageNet. Available online: <https://www.radimagenet.com/> (accessed on January 8, 2024).

138. EyePACS. Available online: <https://paperswithcode.com/dataset/kaggle-eyepacs> (accessed on January 8, 2024).

139. Medical Segmentation Decathlon. Available online: <http://medicaldecathlon.com/> (accessed on January 8, 2024).

140. DDSM. Available online: <http://www.eng.usf.edu/cvprg/Mammography/Database.html> (accessed on January 8, 2024).

141. LIDC-IDRI. Available online: <https://wiki.cancerimagingarchive.net/display/Public/LIDC-IDRI> (accessed on January 8, 2024).

142. Synapse. Available online: <https://www.synapse.org/#!Synapse:syn3193805/wiki/217789> (accessed on January 8, 2024).

143. Mini-MIAS. Available online: <http://peipa.essex.ac.uk/info/mias.html> (accessed on January 8, 2024).

144. Breast Cancer His-to-pathological Data-base (BreakHis). Available online: <https://web.inf.ufpr.br/vri/databases/breast-cancer-histo-pathologi-cal-database-breakhis/> (accessed on January 8, 2024).

145. Messidor. Available online: <https://www.adcis.net/en/third-party/messidor/> (accessed on January 8, 2024).

146. Li, J.; Cheng, Jh.; Shi, Jy.; Huang, F. Brief Introduction of Back Propagation (BP) Neural Network Algorithm and Its Improvement. In *Advances in Computer Science and Information Engineering*; Jin, D., Lin, S., eds.; Springer: Berlin, Germany, 2012, 169, 1–10. [https://doi.org/10.1007/978-3-642-30223-7\\_87](https://doi.org/10.1007/978-3-642-30223-7_87).

147. Johnson, X.Y.; Venayagamoorthy, G.K. Encoding Real Values into Polychronous Spiking Networks. In Proceedings of the International Joint Conference on Neural Networks (IJCNN), Barcelona, Spain, 18–23 July 2010. pp. 1–7. <https://doi.org/10.1109/IJCNN.2010.5596369>.

148. Bohte, S.M.; Kok, J.N.; La Poutre, H. Error-back propagation in temporally encoded networks of spiking neurons. *Neurocomputing* 2002, 48, pp. 17–37. [https://doi.org/10.1016/S0925-2312\(01\)00658-0](https://doi.org/10.1016/S0925-2312(01)00658-0).

149. Rajagopal, S.; Chakraborty, S.; Gupta, M.D. Deep Convolutional Spiking Neural Network Optimized with Arithmetic Optimization Algorithm for Lung Disease Detection Using Chest X-Ray Images. *Biomed. Signal Process. Control.* 2023, 79, 104197. <https://doi.org/10.1016/j.bspc.2022.104197>.

150. Kheradpisheh, S.R.; Ghodrati, M.; Ganjtabesh, M.; Masquelier, T. Bio-Inspired unsupervised learning of visual features leads to robust invariant object recognition. *Neurocomputing* 2016, 205, 382–392. <https://doi.org/10.1016/j.neucom.2016.04.029>.

151. Brader, J.M.; Senn, W.; Fusi, S. Learning real-world stimuli in a neural network with spike-driven synaptic dynamics. *Neural Comput.* 2007, 19, 2881–2912. <https://doi.org/10.1162/neco.2007.19.11.2881>.

152. Masquelier, T.; Guyonneau, R.; Thorpe, S.J. Competitive STDP-based spike pattern learning. *Neural Comput.* 2009, 21, pp. 1259–1276. <https://doi.org/10.1162/neco.2008.06-08-804>.

153. Lee, J.H.; Delbrück, T.; Pfeiffer, M. Training deep spiking convolutional neural Networks with STDP-based unsupervised pre-training followed by supervised fine-tuning. *Front. Neurosci.* 2018, 12, 435. <https://doi.org/10.3389/fnins.2018.00435>.

154. Lee, J.H.; Delbrück, T.; Pfeiffer, M. Enabling Spike-Based Backpropagation for Training Deep Neural Network Architectures. *Front. Neurosci.* 2020, 14, 119. <https://doi.org/10.3389/fnins.2020.00119>.

155. Wu, Y.; Deng, L.; Li, G.; Zhu, J.; Shi, L. Direct training for spiking neural networks: Faster, Larger, Better. In Proceedings of the AAAI Conference on Artificial Intelligence, Honolulu, HI, USA, 27 January–1 February 2019, 33, 1311–1318. <https://doi.org/10.1609/aaai.v33i01.33011311>.

156. Neil, D.; Pfeiffer, M.; Liu, S.-C. Learning to be efficient: algorithms for training low-latency, low-compute deep spiking neural networks. Proceedings of the 31st Annual ACM Symposium on Applied Computing (SAC '2016). Association for Computing Machinery, New York, NY, USA, 293–298. <https://doi.org/10.1145/2851613.2851724>.

157. Lee, J.H.; Delbrück, T.; Pfeiffer, M. Training deep spiking neural networks using backpropagation. *Front. Neurosci.* 2016, 10, 508. <https://doi.org/10.3389/fnins.2016.00508>.

158. Zhan, K.; Li, Y.; Li, Q.; Pan, G. Bio-Inspired Active Learning Method in spiking neural network. *Know.-Based Syst.* 2023, 261, C. <https://doi.org/10.3390/s23052433>.

159. Wang, J.; Chen, S.; Liu, Y.; Lau, R. Intelligent Metaverse Scene Content Construction. *IEEE Access* 2023, 11, 76222-76241. <https://doi.org/10.1109/ACCESS.2023.3297873>.

160. He, S.; Bao, R.; Li, J.; Stout, J.; Bjornerud, A.; Grant, P.E.; Ou, Y. Computer-Vision Benchmark Segment-Anything Model (SAM) in Medical Images: Accuracy in 12 Datasets. *arXiv* preprint arXiv: 2304.09324, 2023; Available online: <https://doi.org/10.48550/arXiv.2304.09324> (accessed on 13 November 2023).

161. Himangi; Singla, M. To Enhance Object Detection Speed in Meta-Verse Using Image Processing and Deep Learning. *Int. J. Intell. Syst. Appl. Eng.* 2023, 11, 176–184. <https://ijisae.org/index.php/IJISAE/article/view/3106>.

162. Pooyandeh, M.; Han, K.-J.; Sohn, I. Cybersecurity in the AI-Based Metaverse: A Survey. *Appl. Sci.* 2022, 12, 12993. <https://doi.org/10.3390/app122412993>.

163. Hirling, D.; Tasnadi, E.; Caicedo, J.; Caroprese, M. V.; Sjögren, R.; Aubreville, M.; Koos, K.; Horvath, P. Segmentation metric misinterpretations in bioimage analysis. *Nat. Methods* 2023 <https://doi.org/10.1038/s41592-023-01942-8>.

164. Pregowska, A.; Perkins, M. Artificial Intelligence in Medical Education: Technology and Ethical Risk 2023; (Available online: November 24, 2023). Available at SSRN: <https://ssrn.com/abstract=576612> (accessed on 24 November 2023).

165. Goutte, C.; Gaussier, E. A Probabilistic Interpretation of Precision, Recall and F-Score, with Implication for Evaluation. In: Losada, D.E., Fernández-Luna, J.M. (eds) Advances in Information Retrieval. ECIR 2005. Lecture Notes in Computer Science, Springer, Berlin, Heidelberg, 3408, 2005. [https://doi.org/10.1007/978-3-540-31865-1\\_25](https://doi.org/10.1007/978-3-540-31865-1_25).

166. Schneider, P.; Xhafa, F. Chapter 3 - Anomaly detection: Concepts and methods, Editor(s): Schneider, P., Xhafa, F. Anomaly Detection and Complex Event Processing over IoT Data Streams, Academic Press, 2022, pp. 49–66. <https://doi.org/10.1016/B978-0-12-823818-9.00013-4>.

167. Nahm, F.S. Receiver operating characteristic curve: overview and practical use for clinicians. *Korean Journal of Anesthesiology* 2022, 75(1), 25–36. <https://doi.org/10.4097/kja.21209>.

168. Perkins N. J.; Schisterman E. F. The inconsistency of “optimal” cut-points using two ROC based criteria. *American Journal of Epidemiology* 2006, 163(7), 670–675. <https://doi.org/10.1093/aje/kwj063>.

169. Pawłowska, A.; Karwat, P.; Żołek, N. Letter to the Editor. Re: “[Dataset of breast ultrasound images by W. Al-Dhabayani, M. Gomaa, H. Khaled & A. Fahmy, Data in Brief, 2020, 28, 104863]”, *Data in Brief* 2023, 48, 109247. <https://doi.org/10.1016/j.dib.2023.109247>.

170. Marcello, S.; Shunra, Y.; Ruggero, M. Neural and axonal heterogeneity improves information transmission, *Physica A: Statistical Mechanics and its Applications* 2023, 618, 12862.

171. Kanwisher, N.; Khosla, M.; Dobs, K. Using artificial neural networks to ask 'why' questions of minds and brains. *Trends Neurosci.* 2023, 46(3):240-254.

172. UNESCO open data. <https://unesdoc.unesco.org/ark:/48223/pf0000385841> (accessed on January 8, 2024).

173. EC AI. <https://digital-strategy.ec.europa.eu/en/library/assessment-list-trustworthy-artificial-intelligence-alta-i-self-assessment> (accessed on January 8, 2024).

174. Radclyffe, C.; Ribeiro, M.; Wortham, R.H. The assessment list for trustworthy artificial intelligence: A review and recommendations. *Front Artif Intell.* 2023, 6. <https://doi.org/10.3389/frai.2023.1020592>.

175. EU AI regulations. <https://www.europarl.europa.eu/news/en/headlines/society/20230601STO93804/eu-ai-act-first-regulation-on-artificial-intelligence> (accessed on January 8, 2024).

176. Pregowska, A. Perkins, M. Artificial Intelligence in Medical Education Part 1: Typologies and Ethical Approaches. Available at SSRN: <https://ssrn.com/abstract=4576612> or <http://dx.doi.org/10.2139/ssrn.4576612> (accessed on 24 November 2023).

177. Adrian, E. D. The impulses produced by sensory nerve endings: Part I. *The Journal of Physiology* 1926, 61(1), 49. <https://doi.org/10.1111/j.physiol.1926.sp002273>.

178. Yao, C.; Tang, J.; Hu, M.; Wu, Y.; Guo, W.; Li, Q.; Zhang, X.-P. Claw U-Net: A UNet-Based Network with Deep Feature Concatenation for Scleral Blood Vessel Segmentation. *arXiv* preprint arXiv:2010.10163, 2020. Available online: <https://doi.org/10.48550/arXiv.2010.10163> (accessed on January 8, 2024).

179. Redmon, J.; Divvala, S.; Girshick, R.; Farhadi, A. You only look once: Unified, real-time object detection. *Proceedings of the IEEE conference on computer vision and pattern recognition* 2016, 779–788.

180. Vaswani, A.; Shazeer, N.; Parmar, N.; Uszkoreit, J.; Jones, L.; Gomez, A.; Kaiser, L.; I. Polosukhin, I. Attention is all you need, *Adv. Neur. Inf. Process Syst.* 2017, 30.

181. Yuan, F.; Zhang, Z.; Fang, Z. An effective CNN and Transformer complementary network for medical image segmentation, *Pattern Recognition* 2023, 136, 109228. <https://doi.org/10.1016/j.patcog.2022.109228>.

182. Dosovitskiy, A.; Beyer, L.; Kolesnikov, A.; Weissenborn, D.; Zhai, X.; Unterthiner, T.; Dehghani, M.; Minderer, M.; Heigold, G.; Gelly, S.; et al., An image is worth 16x16 words: Transformers for image recognition at scale, 2020, arXiv preprint arXiv:2010.11929. (accessed on January 8, 2024)

183. Liu, Z.; Lin, Y.; Cao, Y.; Hu, H.; Wei, Y.; Zhang, Z.; Lin, S.; Guo, B. Swin transformer: Hierarchical vision transformer using shifted windows, in: Proceedings of the IEEE/CVF International Conference on Computer Vision, 2021, pp. 10012–10022.

184. Touvron, H.; Cord, M.; Matthijs, D.; Massa, F.; Sablayrolles, A.; Jegou, H. Training data-efficient image transformers & distillation through attention, in: International Conference on Machine Learning, PMLR, 2021, pp. 10347–10357.

185. Han, K.; Wang, Y.; Chen, H.; Chen, X.; Guo, J.; Liu, Z.; Tang, Y.; Xiao, A.; Xu, C.; Xu, Y. A survey on vision Transformer, IEEE Trans. Pattern Anal. Mach. Intell. 2022, 45(1), 87–110. <http://doi.org/10.1109/TPAMI.2022.3152247>.

186. Mauricio, J.; Domingues, I.; Bernardino, J. Comparing vision Transformers and Convolutional Neural Networks for image classification: A Literature Review. Appl. Sci. 2023, 13, 5521. <https://doi.org/10.3390/app13095521>.

187. Wang, H. Traffic Sign Recognition with Vision Transformers. In Proceedings of the 6th International Conference on Information System and Data Mining, Silicon Valley, CA, USA, 27–29 May 2022; Association for Computing Machinery: New York, NY, USA, 2022; pp. 55–61.

188. Bakhtiarnia, A.; Zhang, Q.; Iosifidis, A. Single-layer vision Transformers for more accurate early exits with less overhead. Neural Networks 2022, 153, 461–473.

189. Chen, J.; Lu, Y.; Yu, Q.; Luo, X.; Adeli, E.; Wang, Y.; Lu, L.; Yuille, A.L.; Zhou, Y. Transunet: Transformers make strong encoders for medical image segmentation, 2021, arXiv preprint arXiv:2102.04306. (accessed on January 8, 2024)

190. Zhou, T.; Li, Q.; Lu, H.; Cheng, Q.; Zhang, X. GAN review: Models and medical image fusion applications, Information Fusion, 2023, 91, 134–148. <https://doi.org/10.1016/j.inffus.2022.10.017>.

191. Son, J.; Park, S.J.; Jung, K.-H. Towards accurate segmentation of retinal vessels and the optic disc in Fundoscopic images with generative adversarial networks. J. Digit. Imaging 2019, 32, 499–512. <https://doi.org/10.1007/s10278-018-0126-3>.

192. Güven, S.A.; Talu, M.F. Brain MRI high resolution image creation and segmentation with the new GAN method, Biomedical Signal Processing and Control, 2023, 80, 104246. <https://doi.org/10.1016/j.bspc.2022.104246>.

193. Skandarani, Y.; Jodoin, P.-M.; Lalande, A. GANs for Medical Image Synthesis: An Empirical Study. J. Imaging 2023, 9, 69. <https://doi.org/10.3390/jimaging9030069>.

194. Hitaj, B.; Ateniese, G.; Perez-Cruz, F. 2017, Deep Models Under the GAN: Information Leakage from Collaborative Deep Learning. 2017, CCS '17: Proceedings of the 2017 ACM SIGSAC Conference on Computer and Communications Security 603–618. doi: 10.1145/3133956.3134012.

195. Jiang, W.; Luo, J. Graph neural network for traffic forecasting: a survey, 2021, <https://arxiv.org/abs/2101.11174>.

196. Liang, F.; Qian, C.; Yu, W.; Griffith, D.; Golmie, N. Survey of Graph Neural Networks and Applications, Wireless Communications and Mobile Computing 2022, ID 9261537. <https://doi.org/10.1155/2022/9261537>.

197. Zhang, L.; Zhao, Y.; Che, T.; Li, S.; Wang, X. Graph neural networks for image-guided disease diagnosis: a review. iRADIOLOGY. 2023; 1(2): 151–66. <https://doi.org/10.1002/ird3.20>.

198. Hamilton, W.; Ying, Z.; Leskovec, J. Inductive representation learning on large graphs. Advances in neural information processing systems 2017 pp. 1024–1034.

199. Ahmedt-Aristizabal, D.; Armin, M.A.; Denman, S.; Fookes, C.; Petersson, L. Graph-based deep learning for medical diagnosis and analysis: past, present and future. Sensors 2021; 21(14):4758. <https://doi.org/10.3390/s21144758>.

200. Chang, X.; Ren, P.; Xu, P.; Li, Z.; Chen, X.; Hauptmann, A. A comprehensive survey of scene graphs: generation and application. IEEE Trans Pattern Anal. Mach. Intell. 2021; 45(1): 1–26. <https://doi.org/10.1109/tpami.2021.3137605>.

201. Ji, S.; Pan, S.; Cambria, E.; Marttinen, P.; Yu, P.S. A survey on knowledge graphs: representation, acquisition, and applications. IEEE Transact Neural Networks Learn Syst. 2021; 33(2): 494–514. <https://doi.org/10.1109/tnnls.2021.3070843>.

202. Scarselli, F.; Gori, M.; Tsoi, A.C.; Hagenbuchner, M.; Monfardini, G. The graph neural network model. IEEE Transactions on Neural Networks 2009, 20(1): 61–80. doi: 10.1109/TNN.2008.2005605.

203. He, P.H.; Qu, A.P.; Xiao, S.M.; Ding, M.D. A GNN-based Network for Tissue Semantic Segmentation in Histopathology Image. Journal of Physics 2023: Conference Series, Volume 2504, The 3rd International Conference on Computer, Big Data and Artificial Intelligence (ICCBDAI 2022) DOI 10.1088/1742-6596/2504/1/012047.

204. Fabijanska, A. graph convolutional networks for semi-supervised image segmentation. IEEE Access 2022, 10, 104144–104155. doi: 10.1109/ACCESS.2022.3210533.

205. Jiang, X.; Hu, Z.; Wang, S.; Zhang, Y. Deep learning for medical image-based cancer diagnosis. Cancers 2023, 15, 3608. <https://doi.org/10.3390/cancers15143608>.

206. Ayaz, H.; Khosravi, H.; McLoughlin, I.; Tormey, D.; Özsunar, Y.; Unnikrishnan, S. A random graph-based neural network approach to assess glioblastoma progression from perfusion MRI. Biomedical Signal Processing and Control 2023, 86, Part C, 105286. <https://doi.org/10.1016/j.bspc.2023.105286>.

207. Evans, L.M.; Sozumert, E.; Keenan, B.E.; Wood, C.E.; du Plessis A. A Review of Image-Based Simulation Applications in High-Value Manufacturing. Arch Comput Methods Eng. 2023, 30, 1495–1552. <https://doi.org/10.1007/s11831-022-09836-2>.

208. Sitzmann, V.; Martel, J. N. P.; Bergman, A. W.; Lindell, D. B.; Wetzstein G. Implicit Neural Representations with Periodic Activation Functions, <https://doi.org/10.48550/arXiv.2006.09661>. (accessed on January 8, 2024)

209. Stolt-Ansó, N.; McGinnis, J.; Pan, J.; Hammernik, K.; Rueckert D.; NISF: Neural Implicit Segmentation Functions, <https://doi.org/10.48550/arXiv.2309.08643>. (accessed on January 8, 2024)

210. Byra, M.; Poon, C.; Shimogori, T.; Skibbe, H. Implicit neural representations for joint decomposition and registration of gene expression images in the <https://doi.org/10.48550/arXiv.2308.04039.marmoset> brain, <https://doi.org/10.48550/arXiv.2308.04039>. (accessed on January 8, 2024)

211. Open data policy UNESCO. <https://www.unesco.org/en/open-solutions/open-data> (accessed on January 8, 2024)